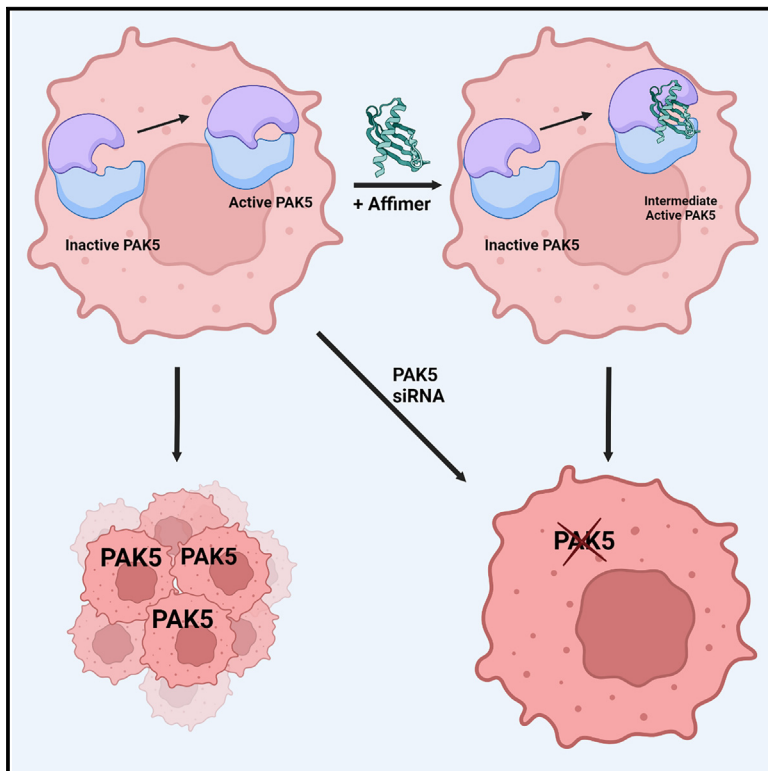


Affimer-mediated locking of p21-activated kinase 5 in an intermediate activation state results in kinase inhibition

Graphical abstract



Authors

Heather L. Martin, Amy L. Turner, Julie Higgins, ..., Margaret A. Knowles, Richard W. Bayliss, Darren C. Tomlinson

Correspondence

d.c.tomlinson@leeds.ac.uk

In brief

Martin et al. report that inhibition of p21 activated kinase 5 (PAK5) leads to G1/S transition arrest, cell enlargement, and reduced cell number. They identify a biologic inhibitor, Affimer 17, which locks PAK5 in a conformation representing an intermediate state of activation resulting in kinase inhibition.

Highlights

- PAK5 siRNA knockdown leads to G1/S arrest, cell enlargement, and reduced cell number
- PAK5 inhibition with biologic, Affimer 17, mimics siRNA knockdown phenotype
- Affimer 17 locks PAK5 in an intermediate activation state resulting in inhibition
- Affimer 17 binding PAK5 Arg653 confers selectivity for PAK5



Article

Affimer-mediated locking of p21-activated kinase 5 in an intermediate activation state results in kinase inhibition

Heather L. Martin,^{1,2,3} Amy L. Turner,^{3,4} Julie Higgins,¹ Anna A. Tang,^{3,4} Christian Tiede,^{3,4} Thomas Taylor,³ Sitthithon Siripanthong,^{3,4} Thomas L. Adams,^{3,4} Iain W. Manfield,^{3,4} Sandra M. Bell,^{1,2} Ewan E. Morrison,^{1,2} Jacquelyn Bond,^{1,2} Chi H. Trinh,^{3,4} Carolyn D. Hurst,² Margaret A. Knowles,² Richard W. Bayliss,^{3,4} and Darren C. Tomlinson^{1,3,4,5,*}

¹BioScreening Technology Group, Leeds Institutes of Molecular Medicine, University of Leeds, Leeds LS9 7TF, UK

²Division of Molecular Medicine, Leeds Institute of Medical Research at St James's University Hospital, University of Leeds, Leeds LS9 7TF, UK

³School of Molecular and Cellular Biology, University of Leeds, Leeds LS2 9JT, UK

⁴Astbury Centre for Structural and Molecular Biology, University of Leeds, Leeds LS2 9JT, UK

⁵Lead contact

*Correspondence: d.c.tomlinson@leeds.ac.uk

<https://doi.org/10.1016/j.celrep.2023.113184>

SUMMARY

Kinases are important therapeutic targets, and their inhibitors are classified according to their mechanism of action, which range from blocking ATP binding to covalent inhibition. Here, a mechanism of inhibition is highlighted by capturing p21-activated kinase 5 (PAK5) in an intermediate state of activation using an Affimer reagent that binds in the P+1 pocket. PAK5 was identified from a non-hypothesis-driven high-content imaging RNAi screen in urothelial cancer cells. Silencing of PAK5 resulted in reduced cell number, G1/S arrest, and enlargement of cells, suggesting it to be important in urothelial cancer cell line survival and proliferation. Affimer reagents were isolated to identify mechanisms of inhibition. The Affimer PAK5-Af17 recapitulated the phenotype seen with siRNA. Co-crystallization revealed that PAK5-Af17 bound in the P+1 pocket of PAK5, locking the kinase into a partial activation state. This mechanism of inhibition indicates that another class of kinase inhibitors is possible.

INTRODUCTION

Cancer is a leading cause of death, responsible for 30% of premature deaths worldwide, a figure that is projected to rise,¹ and it includes 10%–15% of urothelial cancers that are muscle invasive and have a poor 5-year survival rate,² necessitating new therapeutic approaches. However, drug discovery is costly and ineffective, with an average cost of \$1.2 billion and an approximate failure rate of 90%.³ While a large proportion of this failure occurs in human trials, (around 75%),³ a considerable number of promising targets fail as they are not amenable to modulation by small molecules.⁴ Determining a target's druggability and the likely binding sites for small molecules are especially important if the target was identified by RNAi approaches, as these remove a protein from a cellular environment, and this is a process that cannot be replicated efficiently and discretely by small molecules. The development of non-immunoglobulin scaffold-based binding proteins (SBPs) provides a quick and cost-effective way to aid in target validation. SBPs are small proteins, typically in the region of 100–200 amino acids, with a fixed stable scaffold that constrains one or more variable regions.⁵ The introduction of such variability generates libraries of variants from

which one can select for specific binders for a defined target protein, domain, or modification. To date, SBPs based on a variety of different scaffolds have been used as research tools, ranging from crystallization chaperones and antibody replacements to diagnostics and biopharmaceuticals.⁵ SBPs present advantages over other protein-based approaches as they are small proteins that can be easily delivered by standard cell biology techniques, including transient transfection and viral transduction, or even modified to be cell-penetrating proteins.⁶ They function readily in the reducing intracellular environment as they frequently have no cysteine residues.⁷ These are all features of the Affimer technology used in this study,^{8,9} which has been shown to have a number of roles as research tools including the identification of druggable pockets on hard to drug proteins such as RAS.^{10,11} Thus, SBPs provide an orthogonal approach to test the druggability of target proteins identified by RNAi.

A distinguishing feature of tumorigenesis and cancer development is cell-cycle dysregulation,¹² and while major regulators of all the key stages of the cell cycle have been identified, for example the cyclins and cyclin-dependent kinases (CDKs), the detailed regulation of these complex yet fundamental biological processes is not fully understood.¹³ Indeed, recent work



suggests the control of the cell cycle may be tissue specific,^{14,15} and thus the nature of cell-cycle dysregulation may be cancer type specific, a fact that is reflected in the variety of genetic alterations seen in cancer.¹⁴ Determining the genes and proteins involved in this dysregulation in a number of cancers may identify those specific to different cancers and pave the way for novel therapeutics. To achieve this requires an approach that can be easily applied to a wide range of cell types, such as high-content screening, permitting phenological identification of alterations in the cell cycle.^{16–19} Here, we describe a high-content analysis method for identifying the individual phases of the cell cycle that is used in conjunction with RNAi reagents to identify genes, and their correlating proteins, that disrupt the cell cycle and then Affimer reagents to determine if these targets are amenable to small molecule manipulation. Our group has recently demonstrated that Affimer reagents can be used to probe proteins for druggable hotspots and to constrain proteins in conformations that may identify new druggable regions.^{10,11} This highlights their potential not only as binding reagents for different applications^{8–11,20–25} but also their ability to aid in the development of pharmacophores as starting points for drug discovery. For this proof of principle, we undertook small-scale screens focused on a key group of proteins involved in cell-cycle regulation—the protein kinases.^{14,26} All the major checkpoints of the cell cycle and mitosis have specific kinase requirements, notably the CDKs and Polo-like kinase 1 (PLK1).^{27,28} In addition, recent shRNA studies have demonstrated that kinase requirements vary between cancer cell lines in a highly diverse manner.^{29–31}

Here we identify PAK5, as a kinase that has a role in urothelial cancer but not in osteosarcoma, using a protein kinase siRNA library, in conjunction with high-content screening. PAK5 expression regulates cell proliferation via the G1/S transition together with effects on cyclin D1 expression. Based on the knowledge that kinases can be inhibited by a variety of mechanisms, we isolated Affimer reagents against PAK5 and biochemically and structurally characterized the inhibition. The inhibitory Affimer reagent, which recapitulated the siRNA phenotype, locked PAK5 in a conformation not previously reported by binding in the P+1 pocket, giving a DFG-in state, combined with an α C helix-inter conformation, which lacks stable N-terminal extension and inhibits the anchoring of glycine rich loop, and a disassembled R-spine. This is the first structural characterization of a PAK5 inhibitor, showing higher resolution than previously seen with other PAK5 structures. It gives us novel insights into the time-resolved kinase activation sequence that demonstrates potential for application to kinases globally. This, together with the specificity of the Affimer reagent for PAK5 over the other group II PAK proteins, presents exciting opportunities to explore the functions of PAK5 in greater detail and the potential to develop specific small molecule inhibitors to delineate the roles of this kinase from the other PAK family members.

RESULTS

Assay development and screening

An analysis protocol, utilizing high-content imaging, was designed and tested to assign individual cells to specific phases

of the cell cycle to allow the identification of specific kinases that alter proliferation and survival in urothelial carcinoma cells (Figure 1A). Initially U-2 OS osteosarcoma cells were used to permit comparisons with previous studies^{19,32} and to be used as a counter-screen to remove kinases that globally alter cell cycle. Cell-cycle phase was delineated by expression of phase-specific proteins and nuclear morphology (Table S1), with mitotic cells being positive for phosphohistone H3 staining and S-phase cells being positive for EdU staining.³³ Telophase and apoptotic cells were then separated from the remaining cells by size and DAPI intensity and distinguished from each other by distance between nuclei. M-phase cells were calculated as the sum of phosphohistone H3-positive cells and those identified as being in telophase. G0-phase cells were identified as being negative for Ki67 compared with G1 and G2 phase, which were distinguished from one another based on DAPI intensity and number of Ki67 spots,³⁴ with the latter having increased DAPI intensity due to increased DNA content and fewer Ki67 spots.

The analysis protocol was tested by L-mimosine synchronization (Figure 1B) and siRNA targeting, in asynchronous populations, of genes previously reported to disrupt the cell cycle: *PLK1*, *PSMB1*, and *POLA1*.^{35–37} In concordance with previous work utilizing flow cytometry,³⁸ released cells progressed into S phase, with the peak of cells in S phase occurring between 6 and 9 h after release with over 35% of cells in this phase. By 12 h, over 40% of cells were in G2/M phase, with maximal M-phase cells at 15 h (Figure 1B). As cell death is a frequent consequence of cell cycle disruption (Figure 1C), the number of cells per phase was expressed as a percentage of the total cell number. There were variations in the levels of reduction of mRNA of the three test genes, *PLK1*, *PSMB1*, and *POLA1*, following knockdown between 60% and 95%, but all were significant reductions (Student's t tests; non-targeting [NT] vs. *PLK1* $p = 0.0061$, NT vs. *PSMB1* $p = 0.0034$, NT vs. *POLA1* $p < 0.0113$, and NT vs. *CCNE1* $p = 0.0414$; Figure 1D). The effect of gene knockdown on the cell cycle was assessed in both U-2 OS cells used for the screen development and in 5637 urothelial carcinoma cells, as our aim was to explore urothelial cancer-specific kinase requirements and to identify druggable targets (Figures 1E, 1F, and S1). *PLK1* siRNA significantly increased the percentage of cells in M phase and those undergoing apoptosis with a correlating decrease in G2-phase cells (two-way ANOVA with Dunnett's post hoc test $p < 0.001$ for all three phenotypes), as anticipated.³⁵ *PSMB1* siRNA induced a decrease in the percentage of cells in M- and G2-phase cells (two-way ANOVA with Dunnett's post hoc test $p < 0.001$), together with an increase in the percentage of cells in G1 phase (two-way ANOVA with Dunnett's post hoc test $p < 0.001$). This is in contrast to previous work that reported G2 arrest³⁶ but in a different cell type (HeLa cells), and the changes seen here with *PSMB1* siRNA were consistent across test plates using U-2 OS cells. Therefore, despite the differences to previous work,³⁶ *PSMB1* was still utilized as a control with these cells. However, *PSMB1* siRNA did not show a consistent phenotype in 5637 cells and was replaced by *CCNE1* siRNA, which increased the percentage of cells in G0 and G1 phases concurrent with decreases in the remaining

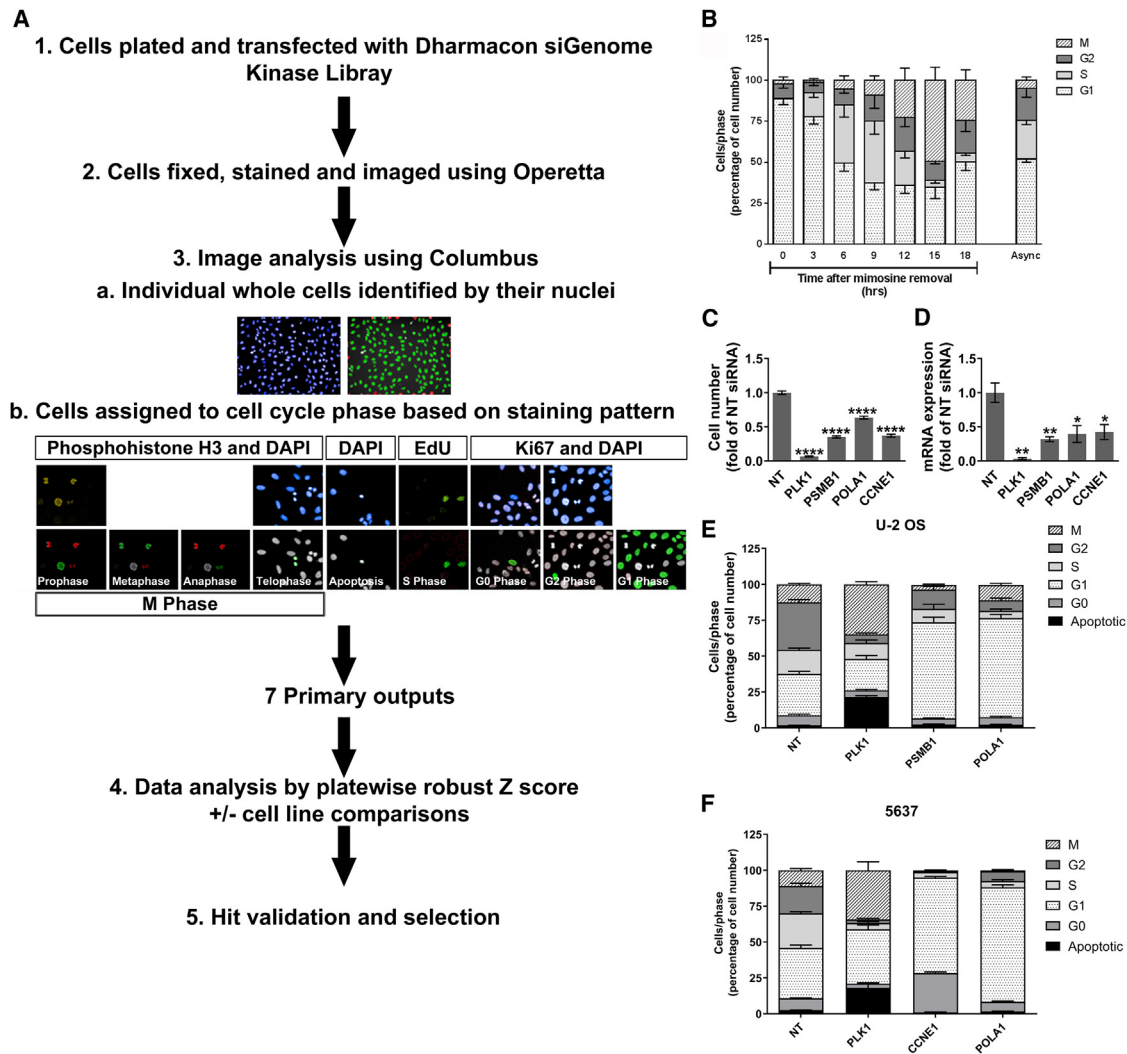


Figure 1. Design and validation of high-content imaging analysis of cell cycle

(A–F) Outline of image generation and analysis, where the key steps in the screening approach to generate high-content images and then their sequential analysis are shown (A). Cells shown in green are positive identifications (see Table S1 for details of the analysis algorithm). Identification of the percentage of cells in each phase of the cell cycle using a novel analysis script in Columbus 2.2 software (PerkinElmer); L-mimosine synchronization induced a G1 block used to validate the analysis script following release of cells to proceed through the cell cycle (B). Effect of 72-h siRNA knockdown on cell number (C). Confirmation of siRNA-induced knockdown of *PLK1*, *PSMB1*, and *POLA1* mRNA (D). Effect of 72-h siRNA knockdown of *PLK1*, *PSMB1/CCNE1*, and *POLA1* on percentage of cells in each cell-cycle phase in U-2 OS osteosarcoma cells (E) and 5637 urothelial carcinoma cells (F) identified with the analysis package. Data are mean \pm SEM, $n = 3$ independent experiments, one-way ANOVA with Dunnett's post hoc test compared to NT. * $p < 0.05$, ** $p < 0.01$, and **** $p < 0.0001$.

phases (two-way ANOVA with Dunnett's post hoc test G0 phase $p < 0.0001$, G1 phase $p < 0.0001$, S phase $p < 0.0001$, G2 phase $p < 0.0001$, and M phase $p < 0.05$). *POLA1* siRNA significantly decreased the percentage of cells in S and G2 phase (as expected for a DNA replication gene³⁷) together with a significant increase in the percentage of G1-phase cells (two-way ANOVA with Dunnett's post hoc test G1 phase $p < 0.0001$, S phase $p < 0.0001$, G2 phase $p < 0.0001$). The reliability of the assay was then assessed by calculation of false positive and false negative rates of 3.22% and 2.58% respectively, from two blind test plates with *PLK1*, *PSMB1*, and *POLA1* siRNA randomly located

across the plate for U-2 OS and 4.12% and 0.52% for two blind test plates containing *PLK1* and *CCNE1* siRNA for 5637 cells. The strictly standardized mean differences for the seven primary outputs (cell number, the percentage of cells in G0, G1, S, G2 and M phase, and the percentage of apoptotic cells) using the appropriate controls for the individual phenotypes were also calculated (Table S2). The analysis protocol was then used to assess the changes in the cell cycle in combination with the Dharmacon siGENOME SMARTpool kinase library consisting of pools of four siRNAs targeting 719 different kinases. The screen was run in duplicate for the U-2 OS counter-screen and triplicate for the target cancer

Table 1. The 16 validated hits specific to 5637 urothelial carcinoma cells

Gene symbol	Gene name	Phenotype						
		Cell number	Apoptosis	G0	G1	S	G2	M
CALM2	calmodulin 2		+					
CDKN2C	cyclin-dependent kinase inhibitor 2C		+					
CRKL	v-crk avian sarcoma virus CT10 oncogene homolog-like		+			–		
CSNK1A1	casein kinase 1, alpha 1		+					
DMPK	dystrophia myotonica-protein kinase						–	
DYRK1A	dual-specificity tyrosine-(Y)-phosphorylation-regulated kinase 1A					–		
EEF2K	eukaryotic elongation factor-2 kinase	–						
HIPK3	homeodomain interacting protein kinase 3	–	+					+
HUNK	hormonally upregulated Neu-associated kinase	–	+					
PAK5	p21 protein (Cdc42/Rac)-activated kinase 5	–					–	
PDGFRA	platelet-derived growth factor receptor, alpha polypeptide					+		
PIK3R4	phosphoinositide-3-kinase, regulatory subunit 4		+					
PIP5K1A	phosphatidylinositol-4-phosphate 5-kinase, type I, alpha	–						
TK2	thymidine kinase 2, mitochondrial					+		
TP53RK	TP53 regulating kinase							+
TYRO3	TYRO3 protein tyrosine kinase		+					+

+, percent of cells in phase increased; –, percent of cells in phase decreased.

cell line 5637, with *PLK1*, *PSMB1/CCNE1*, and *POLA1* (two wells/plate) as positive controls and non-targeting siRNA as the negative control (eight wells/plate).

Identification of urothelial cancer-specific cell-cycle regulators

Plate-wise robust Z scores of greater than two median absolute deviations away from the plate median³⁹ in both screens (U-2 OS and 5637 cells) were used in hit identification. This identified a total of 230 evenly distributed siRNAs (including well-characterized cell cycle controllers such as the CDKs) that altered one or more of the phenotypic outputs for U-2 OS cells and 177 for 5637 cells, of which 101 had not been detected in the U-2 OS screen and were considered more likely to be urothelial cancer-specific hits. (Table S3). These 101 hits were taken forward for further validation using siRNAs with different chemistry and sequences (ON-TARGET plus). Three well-known oncogenes (*RelA*, *Ret*, and *Src*) were removed, and two further genes (*BAIAP1* and *MGC4796*) did not have alternative chemistries available, leaving 96 hits to be taken forward for validation. The 16 hits that were successfully validated (Table 1) were then tested in a panel of urothelial carcinoma cells to identify those with more general impacts on cell cycle in urothelial carcinoma. This reduced the number to four hits (*DYRK1A*, *PAK5*, *PDGFRA*, *TP53RK*) from which *PAK5* was selected for further analysis as *PAK5* knockdown reduced the percentage of cells in S phase together with a reduction in cell number without inducing apoptosis, as opposed to a single phenotype identified for the other three hits.

PAK5 knockdown induces G1/S arrest concurrent with reduced cell number and increased cell size

PAK5 siRNA-induced knockdown significantly reduced cell number by 21%–70% in three different urothelial carcinoma cell lines: 5637, SD, and LUCC3 (one-way ANOVA with Dunnett's post hoc test 5637 $p \leq 0.005$, SD $p = 0.034$, LUCC3 $p = 0.0014$; Figure 2A). This was concurrent with a reduction of the percentage of cells in S phase in 5637 and LUCC3 cell lines (one-way ANOVA with Dunnett's post hoc test 5637 $p \leq 0.002$, SD $p = 0.6105$, LUCC3 $p = 0.0058$; Figures 2B and 2C). Protein levels of *PAK5* were significantly reduced to 40% of those of the controls at the 72-hr time point used in the screen, and this reduction continued at 96 h (one-way ANOVA with Dunnett's post hoc test 72-h $p = 0.0051$, 96-h $p = 0.0099$; Figure 2D). The reduction in cell number seen in the screen was determined to be a result of a reduction in growth rate that was significant after 72 h (two-way ANOVA with Tukey's post hoc test 72-h $p < 0.0001$, 96-h $p < 0.0001$; Figure 2E). During these experiments, it became apparent that *PAK5* knockdown increased nuclear size, and further investigation showed that cell area, as measured by both wheat germ agglutinin Alexa Fluor 633 and phalloidin staining, was also significantly increased (one-way ANOVA with Tukey's post hoc test 72-h $p < 0.0001$, 96-h $p < 0.0001$; Figures 2F, 2G, and 2H). As these data implied a G1/S arrest, we next examined the levels of cyclin D1 as a key regulator of the G1/S transition and also as an indicator of senescence,⁴⁰ as the phenotype of increased cell size was suggestive of senescence.⁴¹ Cyclin D1 protein levels were significantly reduced by

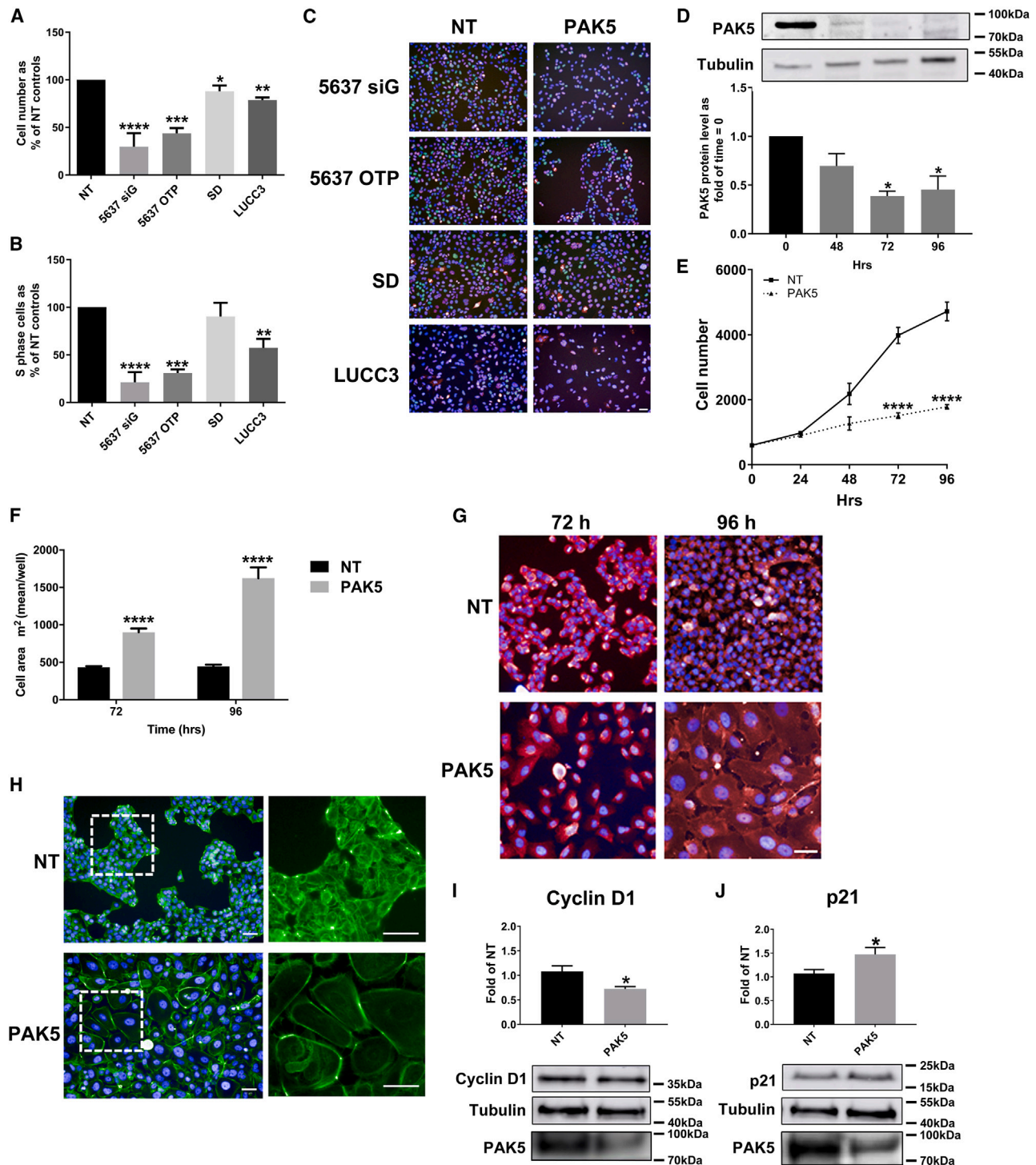


Figure 2. Effects of PAK5 knockdown with SMARTpool siRNA on urothelial carcinoma (5637) cells

(A–J) PAK5 knockdown reduces cell number in a range of urothelial carcinoma cell lines (A) and the percentage of cells in S phase (B) when compared to NT siRNA after 72 h, with representative images shown in (C). Blue, DAPI; green, EdU; yellow, phosphohistone H3; red, Ki67. Time course analysis of PAK5 knockdown in 5637 cells shows reduced PAK5 protein levels by 72 h post transfection (D) (a representative blot is shown). Reduced PAK5 protein levels are concurrent with significant reductions in cell number at both 72 and 96 h post transfection (E). PAK5 knockdown increases cell size at both 72 and 96 h post transfection compared to NT siRNA (F) (mean cell size/well analysis for wheat germ agglutinin Alexa Fluor 633 staining shown). Representative images are shown in (G) (blue,

(legend continued on next page)

PAK5 knockdown in 5637 cells (unpaired t test $p = 0.0155$; [Figure 2I](#)). Levels of p21 were also assessed, the induction of senescence was suggested, and it showed a slight but significant increase (unpaired t test $p = 0.0471$; [Figure 2J](#)). However, when we examined the expression of β -galactosidase as a marker of senescence, we saw minimal expression (less than 5% of cells in all groups), suggesting the increase in cell area was not related to the induction of senescence. The images of F-actin filaments used in the exploration of cell size appear to show altered actin arrangement, and disruption of actin filaments has been reported to lead to G1 arrest concurrent with reductions in cyclin D1 levels.^{42,43} However, further studies are required to explore the potential changes in actin seen with PAK5 knockdown and how these are related to reductions in cyclin D1 and G1 arrest or whether they are instead a downstream effect of the arrest.

Identification of PAK5-binding Affimers that recapitulate PAK5 siRNA knockdown

To continue our assessment of the utility of siRNA screening in conjunction with Affimer technology as a strategy to accelerate drug discovery, we isolated Affimers against the C terminus of PAK5, which incorporates the kinase domain (amino acids 426–719). This led to the isolation of 20 unique Affimers that could bind PAK5 C terminus. A kinase assay was used to determine which PAK5-binding Affimers displayed inhibitory effects by assessment of phosphorylation of BAD (BCL2 Associated Agonist Of Cell Death) at S112, a known target of PAK5⁴⁴ ([Figures 3A, 3B, and S2](#)). Half of the PAK5-binding Affimers reduced phosphorylation of BAD when used at molar ratio of 0.54 to the amount of enzyme (PAK5 kinase domain). The pool of PAK5-binding Affimers was also subjected to phage ELISA screen against the kinase domains of all of the group II PAKs ([Figure 3C](#)), as they have 80% and 84% homology with PAK6 and PAK4, respectively.⁴⁵ Utilizing these data, four Affimers were selected for further testing; PAK5-Af3, PAK5-Af4, PAK5-Af12, and PAK5-Af17. Three of these showed higher specificity for PAK5 over the other group II PAKs, while PAK5-Af12 showed a higher degree of cross-reactivity to PAK6 but was the most effective inhibitor of BAD phosphorylation, showing a 2-fold reduction compared to kinase alone when used at molar ratio of 0.54 to PAK5. The ability of PAK5-binding Affimers to interact with PAK5 in a cellular environment was confirmed using lysates from cells expressing a GFP-tagged PAK5 ([Figure 3D](#)). All four PAK5-binding Affimers selected for further experiments were able to isolate PAK5-GFP from 5637 lysates, while the control Affimer (that binds yeast SUMO protein) did not.

To test the ability of the selected PAK5-binding Affimers to recapitulate PAK5 siRNA knockdown data in cells, we transiently transfected 5637 cells with pCMV6-PAK5-bindingAffimer-tGFP plasmids. Transfection efficiency was 70%–80% and did not significantly vary between the PAK5-binding Affimers or a control Affimer (one-way ANOVA $p = 0.6438$). There appears to be some nuclear localization of GFP signal possibly caused by

GFP as has been previously seen⁴⁶ ([Figure 4A](#)); however this does not significantly differ between the PAK5-binding Affimers and the control Affimer (one-way ANOVA $p = 0.0903$). The three Affimers that showed specificity for PAK5 (PAK5-Af3, PAK5-Af4, and PAK5-Af17) all significantly reduced the number of cells in S phase ([Figure 4B](#)). However, only PAK5-Af17 recapitulated other aspects of the PAK5 siRNA knockdown phenotype showing a similar reduction in cell number of 65.3% (one-way ANOVA with Dunnett's post hoc test $p = 0.0026$; [Figure 4C](#)) and an increase in cell area of 47.8%, as measured by both wheat germ agglutinin and phalloidin staining (one-way ANOVA with Dunnett's post hoc test $p = 0.0049$; [Figures 4D, 4E, and 4F](#)). The latter is considerably less than the 363.5% seen with siRNA knockdown. PAK5-Af17 decreased cyclin D1 protein levels in line with that seen with the siRNA knockdown (unpaired t test $p = 0.0175$; [Figure 4F](#)), while p21 protein levels were increased albeit non-significantly (unpaired t test $p = 0.1311$; [Figure 4G](#)). Thus PAK5-Af17 recapitulates the key features of the PAK5 siRNA knockdown.

PAK5-Af17 locks PAK5 in an intermediate activation state

To further explore the mechanism of inhibition of PAK5 activity by PAK5-Af17, we determined the crystal structure of PAK5-Af17 in complex with the kinase domain of PAK5 at a resolution of 1.55 Å. The asymmetric unit contained one complex of PAK5:PAK5-Af17 (one PAK5 and one Affimer 17 molecule) at a 1:1 stoichiometry, with no magnesium ions or nucleotides (PDB: 8C12). The atomic model revealed that PAK5-Af17 interacts with both the N- and C-lobes of the kinase domain, burying a 665.7-Å interface area across the α C-helix, P+1 region of the activation loop, and the α G-helix.⁴⁷ Thus, PAK5-Af17 binds across the substrate binding region, outside the ATP binding pocket, and is therefore the first non-type I inhibitor of PAK5 ([Figures 5A and 5B](#)). This binding of PAK5-Af17 locks PAK5 in an intermediate inactive conformation, harboring incomplete hallmarks of an active kinase, despite the presence of activating phosphorylation on the activation loop. The α C-helix maintains the salt bridge between Glu494 and Lys478, and the C-terminal turn is distorted, extending the α C- β 4 loop akin to the purine-bound state of the protein.^{48,49} The DFG motif resides in the “in” conformation with the central Phe587 occupying the hydrophobic pocket between the N- and C-lobes⁴⁹ ([Figure S3A](#)). Ser602 of the activation loop is monophosphorylated, and the active H-bond network between Arg600, Arg567, Tyr620, and Phe589 is maintained, linking either end of the activation segment via the catalytic Arg567 residue and stabilizing a conformation still suitable for substrate binding⁴⁸ ([Figure S3B](#)).

Nevertheless, the hydrophobic regulatory R-spine composed of RS1 (His566), RS2 (Phe587), RS3 (Met498), and RS4 (Met509), which has been extensively described as “linear” in the active, ATP-, or substrate-bound state of other kinases,⁵⁰ is clearly distorted in our PAK5 structure, showing a back-pocket-accessible

DAPI; red, wheat germ agglutinin Alexa Fluor 633) and (H) (blue, DAPI; green, phalloidin). PAK5 knockdown downregulates cyclin D1 (I) and upregulates p21 expression (J) at 96 h post transfection. Data are mean \pm SEM, $n = 3$ independent experiments for all panels, one-way ANOVA with Dunnett's post hoc test in (A), (B), and (E), one-way ANOVA with Tukey's post hoc test in (F), and unpaired t test in (I) and (J). NT, non-targeting; siG, siGENOME; OTP; ON-TARGETplus. Scale bars represent 50 μ m. * $p < 0.05$, ** $p < 0.01$, *** $p < 0.001$, and **** $p < 0.0001$.

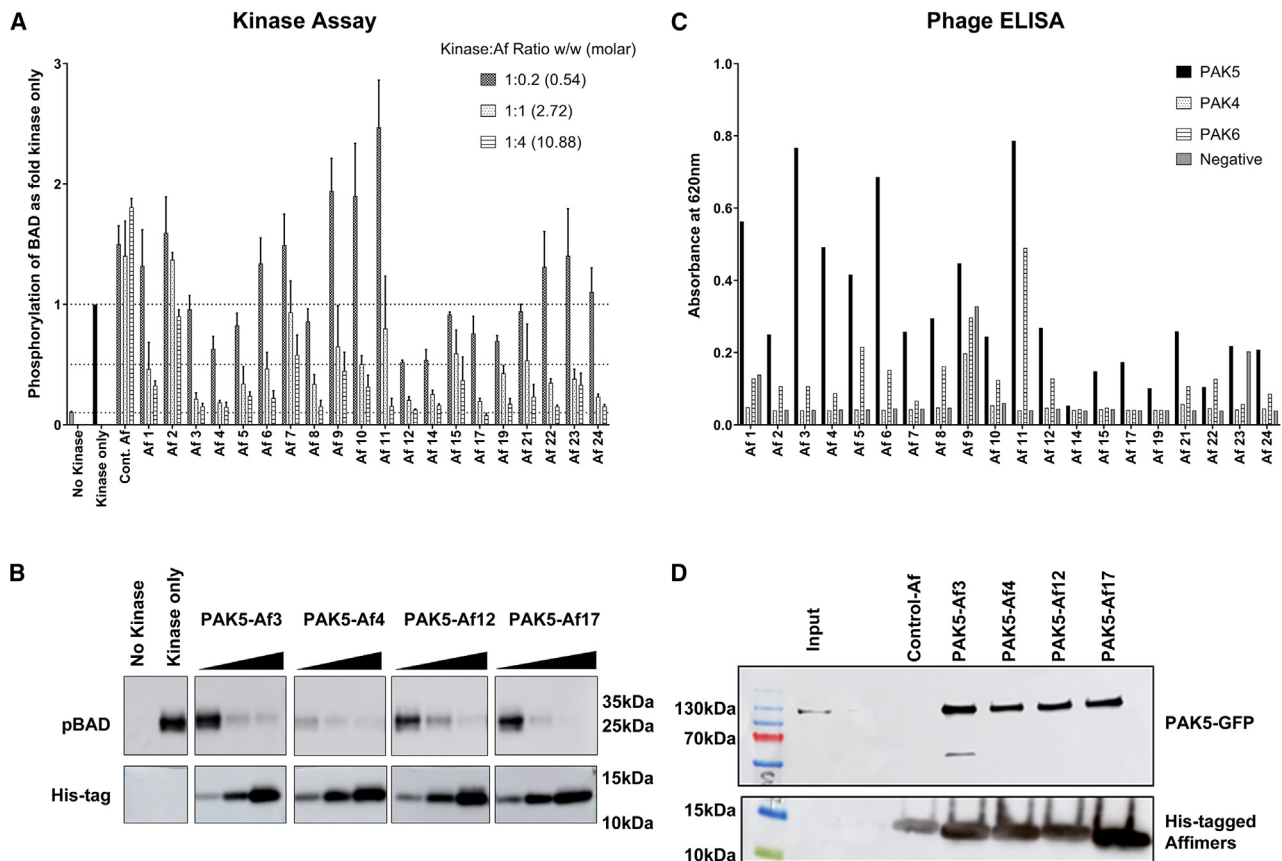


Figure 3. Identification and characterization of PAK5-binding Affimers

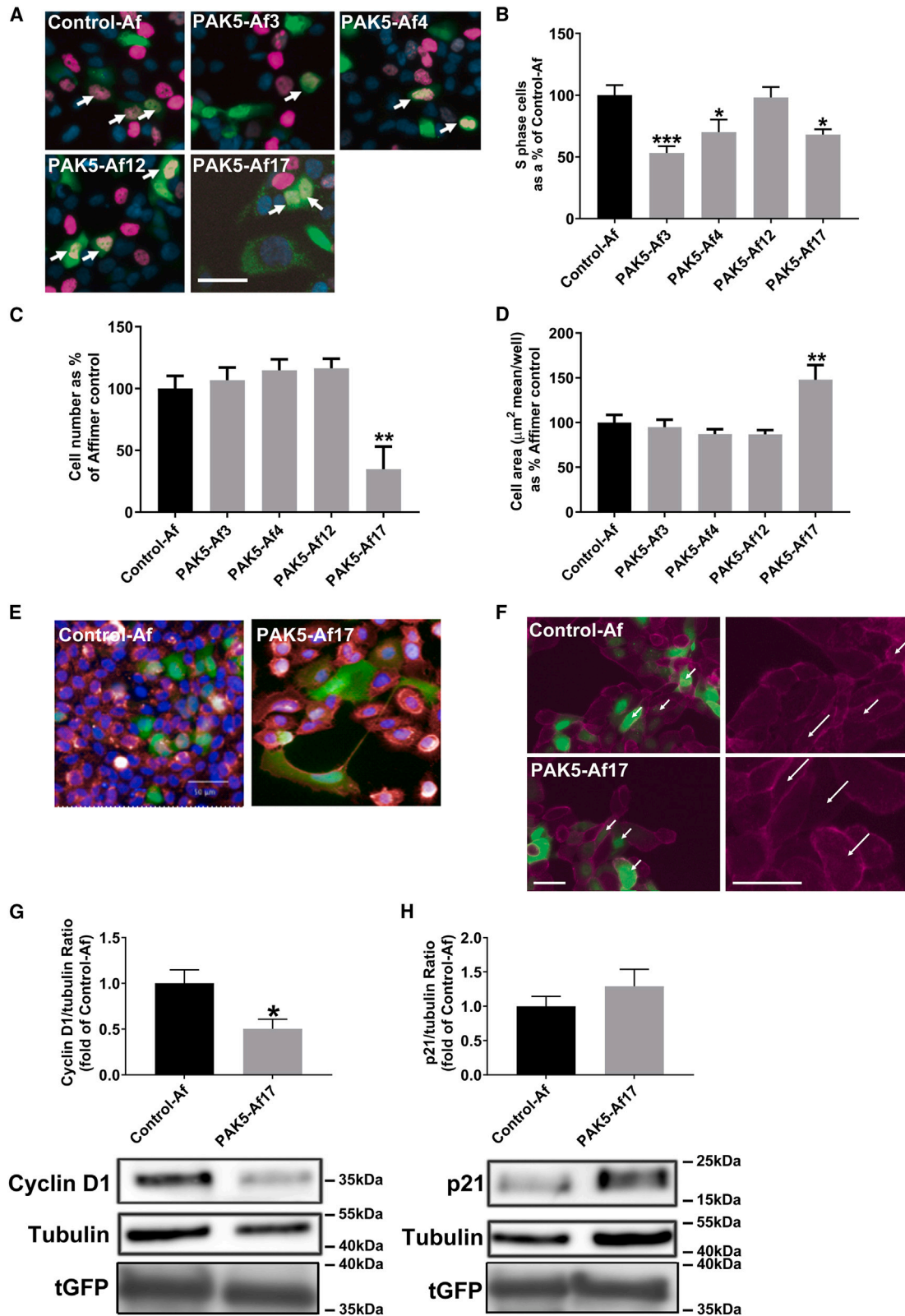
(A–D) The ability of the 20 PAK5-binding Affimers to inhibit PAK5-mediated phosphorylation of BAD was assessed by *in vitro* kinase assay at different w/w ratios and compared to a control Affimer (that binds yeast SUMO protein) (A) ($n = 3$ independent experiments). Data are mean \pm SEM. Representative blots for the four Affimers selected for further characterization (see text for details) are shown in (B). Intermediate lanes showing Affimers not selected have been removed (see Figure S2 for full membranes). The group II PAK binding preferences of the 20 unique Affimers that bind PAK5 kinase domain identified from screening the Affimer phage library (C) were assessed by a phage ELISA screen ($n = 1$). His-tagged PAK5-binding Affimers can pull down PAK5-GFP from 5637 cell lysates (D) (representative blot of three independent experiments).

conformation akin to the inactive PAK4 structure (PDB: 4XBU)⁵¹ (Figure 5C). Moreover, the conserved Glu-Lys salt bridge, although present, is shifted from the position observed in active kinase structures (Figure 5D), and the N-terminal turn of the α C-helix does not extend comparative to the active rearrangement, with length and distortion added to the β 3- α C loop.⁴⁸ The α C-helix is subsequently shortened and has two distorted termini that become loop regions compared to their helically structured counterparts in either the published purine-bound or unbound conformations (PDB: 2F57) (Figure 5E). The α C-helix resembles that of another SBP-kinase complex, the vNAR-D01 bound Aurora A kinase structure (PDB: 5L8L) (Figure S3C) with regard to the number of turns, but it is distinct in its maintenance of the Glu-Lys salt bridge.⁵² This is consistent with the vNAR-D01 and PAK5-Af17 having distinct binding sites and allosteric mechanisms. The completion of the activating N-terminal turn is inhibited by the cation pi interaction of Arg487 with the Affimer VR1 residue Tyr44. Tyr44 further forms an H-bond with Leu603 of the activation loop (Figure 5F). Consequently, this conserved Arg487 is not incorporated into the N-terminal turn and cannot

swing and anchor the glycine rich loop through its activating H-bonding network between Ser459, Gly458, and Glu457. The glycine rich loop is therefore anchored in a partially open conformation stabilized by an H-bond between Thr460 and the conserved Gln485 of the β 3- α C loop. This is a previously unseen conformation of the PAK5 glycine-rich loop (Figure 5G).

The previously described purine-bound PAK5 structure (PDB: 2F57) notes the H-bond anchoring of Asn493 of the α C-helix, with the conserved Cys590 of the activation segment, and Gly588 of the DFG motif.⁴⁸ Although the Affimer-constrained PAK5 shows the DFG-in conformation, accompanied by an intermediate variant of the α C-helix-in conformation (α C-helix-inter), we do not see this linking of key structural elements in the presence of PAK5-Af17. Given this, and the inhibition of the swinging of Arg487 toward the glycine-rich loop, PAK5-Af17 can be considered to freeze PAK5 in a potentially physiologically relevant state, showing clear evidence of the time-resolved point at which activating dynamics were inhibited.

Therapeutically targeting allosteric sites as opposed to ATP-competitive sites is an attractive avenue in the development of



(legend on next page)

more selective kinase inhibitors. As the ATP binding sites across the kinome show high levels of conserved homogeneity, off-target effects are prevalent within the clinical setting.⁵³ PAK5-Af17 binds PAK5 with nanomolar affinity ($K_D = 45 \pm 6.14$ nM) as measured by surface plasmon resonance and appears to display remarkable specificity within the group II PAKs, which share upward of 80% homology, as seen in the phage ELISA screen (Figure 3C). This specificity is facilitated by the Affimer VR2 Pro77 and backbone residue Glu37 forming dynamic H-bonds to Arg653 of the α G-helix of PAK5. Arg653 is unique to PAK5, occupied by a lysine in the other group II PAK proteins and a tyrosine in group I PAK proteins (Figure 5H).⁴⁸ To test the importance of this residue for determining the PAK5-Af17 binding ability to PAK5 and to a lesser extent PAK4 and PAK6, we mutated the corresponding residues in PAK4 and PAK6 to arginine to reflect the situation seen in PAK5. The ability of PAK5-Af17 to bind these mutated versions was then assessed by phage ELISA. In contrast to our phage ELISA screen (Figure 3C) we utilized BAP-tagged versions of the group II PAK proteins to minimize any orientation issues. PAK5-Af17 still showed higher specificity to PAK5 over PAK4 and PAK6 (one-way ANOVA with Dunnett's post hoc test $p = 0.0021$ and $p = 0.0015$ for PAK4 and PAK6 vs. PAK5 respectively; Figure 5I), however a higher degree of binding to these proteins was seen compared with our phage ELISA screen. Mutation of Lys526 (PAK4) and Lys610 (PAK6) to arginine led to increased binding of PAK5-Af17 to these proteins to levels that were not significantly different to PAK5. These results were also replicated by the ability of the different group II PAK proteins to pull down PAK5-Af17, with PAK5 showing the greatest degree of binding, negligible binding PAK4, and some binding to PAK6. Mutation of Lys526 and Lys610 to arginine again increased the binding of PAK5-Af17, but not to the same degree as seen in the phage ELISA (Figure 5J). Thus binding of PAK5-Af17 to Arg653 confers the specificity seen toward PAK5 over the other group II PAKs; indeed all the other interactions PAK5-Af17 makes with PAK5 are with conserved residues within the group II PAKs.⁴⁸

DISCUSSION

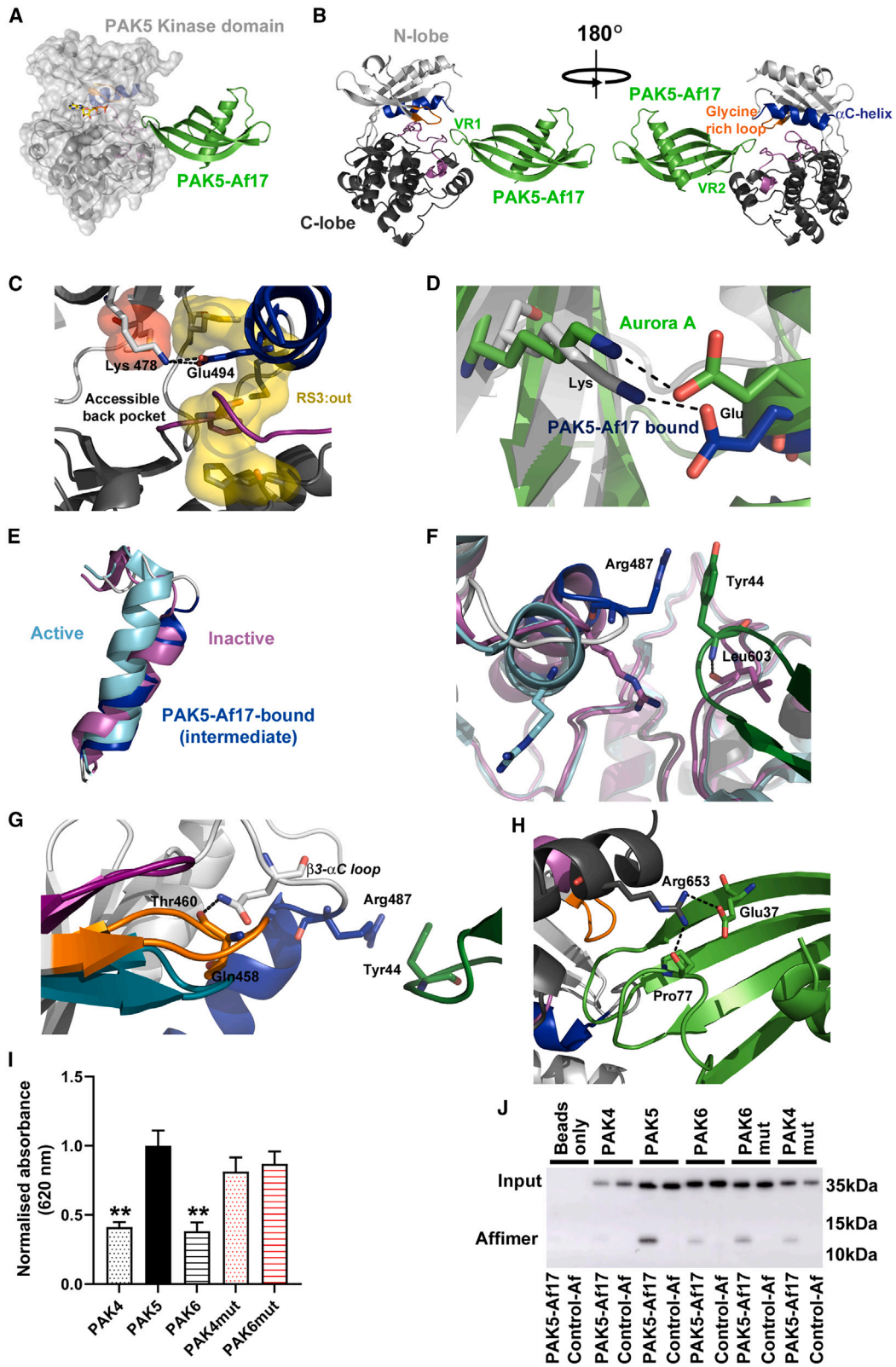
Here, we have presented a high-content screen using siRNA technology that, in combination with Affimer reagents, has the potential to identify targets in a cancer-specific manner. The screen used here utilizes well-known markers of key cell-cycle phases^{16,17,32,33} but with the addition of staining for Ki67, which allows the identification of cells that are not actively dividing G0 cells³⁴ only seen in one previous study.³² This is an important subpopulation in cancer as it can drive recurrent disease.⁵⁴ An

ability to identify this population and the key proteins that induce its formation may offer alternative therapeutic avenues. In addition, the use of a simple immunohistochemistry approach compared with live-cell imaging using cells expressing fluorescently tagged proteins³⁶ or the generation of stable cell lines means this assay is readily adaptable to a wide variety of cell lines and potentially primary cells as well. The screening protocol robustly identified several well-characterized regulators of the cell cycle including CDK1, PLK1, WEE1, CHEK1, and Aurora kinase A (AURKA),^{27,28,55–58} all of which are already known therapeutic targets in cancer, providing confidence that other targets identified by the screening process would have important roles in cancer development and progression. Indeed, PAK5 identified here has previously been shown to have roles in a variety of cancers.^{59–67} The fact that PAK5 has been associated with cancers other than urothelial cancer shows that the approach used here is only as good as the number of counter-screens performed. In the case of PAK5 in this study, this was only a single screen, that of the U-2 OS cells used in assay development. All that can, therefore, be concluded is that PAK5 is involved in urothelial cancer but not potentially in osteosarcoma. Although beyond the scope of this study, if the number of cancer cell types used for counter-screens was increased, highly cancer-type-specific data could be identified.

PAK5 has previously been shown to be upregulated in cancers ranging from glioblastoma to ovarian cancer,^{59–67} suggestive of a more global role for PAK5 in cancer. Only one of these studies⁶⁶ explored the role of PAK5 in urothelial carcinoma, and that focused on its role in E-cadherin-mediated cell-cell adhesion in cell lines representing a variety of grades of urothelial carcinoma with PAK5 levels inversely correlating with grade. This is compatible with the present study as 5637 cells showed epithelial morphology and expressed detectable PAK5. However, the mutational background of the cell lines used by Ismail et al.⁶⁶ and in this study vary,⁶⁸ so comparisons should be made lightly. Both our work and that of Ismail et al.¹¹ support an important role for PAK5 in urothelial carcinoma that requires further exploration. The data in this study also support a more global role for PAK5 in the G1/S transition as previously seen in breast, gastric, and hepatocellular carcinomas,^{59,65,67} where alterations to cyclin D1 levels were also recorded. The mechanism by which PAK5 affects the G1/S transition is currently unclear with NF- κ B-p65,⁶⁵ apoptosis-inducing factor,⁶⁹ cyclin D1, CDK2, and CDC25A⁵⁹ all implicated to date. Our data support a role for alterations to cyclin D1 levels as we saw significant reductions in cyclin D1 levels. It is possible that this reduction is mediated via changes to the actin cytoskeleton⁷⁰ as disruption of actin filaments has been linked to G1 arrest and cyclin D1

Figure 4. Effects of PAK5-binding Affimers in 5637 cells

(A–H) tGFP tagged PAK5-binding Affimers and control Affimers (green) were transfected in 5637 cells and stained with EdU (pink) and DAPI (blue) 24 h after transfection, with representative images shown in (A); arrows indicate GFP- (green) and EdU- (pink) positive cells. PAK5-Af3, PAK5-Af4, and PAK5-Af17 reduce the percentage of cells in S phase compared to the control Affimer (B). PAK5-Af17 transfection also reduces 5637 cell number (C) and increases cell size (D) (mean cell size/well analysis for wheat germ agglutinin Alexa Fluor 633 staining shown), with representative images shown in (E) (blue, DAPI; green, GFP; and red, wheat germ agglutinin Alexa Fluor 633) and (F) (blue, DAPI; green, GFP; and red, phalloidin, with Affimer-expressing cells arrowed for comparison). PAK5-Af17 downregulates cyclin D1 expression (G) and does not significantly affect p21 expression (H) (representative blots shown). Data are mean \pm SEM, $n = 3$ independent experiments for all panels, one-way ANOVA with Dunnett's post hoc test in (B), (C), (D) and unpaired t test in (G) and (H). Scale bars represent 50 μ m. * $p < 0.05$, ** $p < 0.01$, *** $p < 0.001$, and **** $p < 0.0001$.



(legend on next page)

expression.^{42,71} It will be interesting to further explore the role of PAK5 in regulating both G1/S transition and the actin cytoskeleton, which is known to be regulated by PAK proteins,⁷² and whether these two processes are linked.

The ability of the Affimer reagents described here to recapitulate the G1/S arrest and previously^{59,65,67} with PAK5 knockdown supports their use to influence the decision of whether a target is likely to be druggable. However, the magnitude of change was lower with PAK5-Af17 than PAK5 knockdown. This is, most likely, a reflection of the degree of inhibition of PAK5 within the cells, as PAK5 knockdown will remove the majority of PAK5 protein molecules, while PAK5-Af17 may only inhibit a percentage of them, resulting in the less pronounced phenotypes seen. The same reasoning may underlie the differences in p21 levels as this is an upstream regulator of PAK5 reacting to the presence/absence of PAK5. The work presented in this study identified those Affimers able to bind the kinase domain of PAK5, and in a cellular situation, full-length PAK5 with an auto-inhibitory domain and an ability to dimerize is present.⁷³ Additionally the variable regions of PAK5-Af3 and PAK5-Af4 share a degree of sequence homology with known substrate motifs for group II PAKs, notably two basic amino acids, then two or three variable amino acids before an aromatic amino acid,⁷⁴ so they may be in direct competition with *in vivo* substrates in cells that is not seen in the *in vitro* kinase assay. These differences may underlie the differential effects of the Affimers in cells. Thus, the ability of PAK5-Af17 to reproduce the main features of PAK5 knockdown is important in the assessment of its druggability, as it shows inhibition rather than removal of PAK5 can have the same phenotypic effect as would be achieved by small molecule inhibitors.

Like other kinases, the challenge of achieving drug specificity remains with the PAK family, owing in part to their highly conserved ATP binding cleft. There are established pan-kinase targeting ATP-competitive inhibitors that have been shown to abrogate PAK family activity: for example, staurosporine showed an IC₅₀ of 0.6 nM against the group I PAK1.⁷⁵ However, very few PAK selective inhibitors have been reported. The first PAK family-specific inhibitor to enter clinical trials was PF-3758309.⁷⁶ This ATP-competitive compound, originally characterized against PAK4, showed equipotent activity against the other group II PAKs (~20 nM) and to a lesser extent the group I PAKs (~100–200 nM). Unfortunately, PF-3758309 was redacted

from clinical trials after reports of low oral bioavailability, grade 4 neutropenia, and gastrointestinal disorder.⁷⁷ Given this, and as the PAKs adopt a typical kinase fold, allosteric approaches are an attractive therapeutic avenue that could provide more selective cancer treatments, and these have been explored with some success. For example, IPA-3 was shown to bind the auto-inhibitory domain of PAK1 and act as a group I selective inhibitor.⁷⁸ Staben et al.⁷⁹ identified a group II selective compound that bound in the back pocket, thus also displaying intergroup selectivity but not intragroup. Novartis developed the first allosteric PAK inhibitors that showed PAK1 selectivity and that bind in the back pocket of the kinase domain.⁸⁰ This was the first PAK targeting series that showed intragroup selectivity. To date, only one molecule has shown PAK5 specificity over the other PAK family members. PRT062607, a spleen tyrosine kinase (SYK) inhibitor, showed off-target PAK5 inhibition selectivity,⁸¹ but little else is known about its mechanism of action. Thus, the need for selective inhibitors of the individual PAK family members remains. An endogenous inhibitor peptide Inka1 has been reported to inhibit PAK4 by binding in a similar location to PAK5-Af17 (Figure S3D),⁸² but this is postulated to have activity across the group II PAKs. Therefore, the PAK5-Af17:PAK5 crystal structure determined here is, to our knowledge, the first structure of PAK5 in complex with a non-type I inhibitor (ATP mimic),⁵⁰ which shows significant specificity within the group II PAKs delivered by binding to the PAK5 unique residue Arg653. PAK5-Af17 is the first biologic inhibitor described for PAK5 and indeed the first exogenous biologic targeting the PAK family. The PAK5-Af17-bound PAK5 is locked in an intermediate active conformation; thus the classification of this inhibition is somewhat convoluted, although clearly not a type I or II inhibitor that binds the ATP site or bivalent type V or covalent type VI inhibitor.⁶⁷ As the loops bind distal to the ATP binding site, with interactions shown across the N- and C-lobes of the kinase domain within the P+1 site clearly overlapping with other kinase substrates, e.g., N-Myc (Aurora A kinase substrate), and the endogenous inhibitor peptide Inka1 (PAK4 substrate inhibitor), PAK5-Af17 cannot be referred to as type IV.^{82,83} Thus, PAK5-Af17 is most appropriately classified as a type III inhibitor, with the α C-helix adopting an atypical conformation but no direct interaction with the Phe side group of the DFG motif, potentially providing evidence for a novel subclass of type III inhibitor. By

Figure 5. PAK5-Af17 is a non-type 1 inhibitor of PAK5 that locks PAK5 in an intermediate conformation between active and inactive

(A–J) PAK5-Af17 (green) binds at the hinge region between the N lobe (light gray) and C lobe (dark gray) of PAK5. The Affimer is shown to complex with PAK5 at the apex of the activation loop (purple), α C helix (blue), and glycine-rich loop (orange) via both variable regions (VRs) (PDB: 8C12). This site is distinct from the nucleotide binding site, as shown by the overlaid ADP nucleotide from PAK3 (yellow by element; PDB: 6FD3) in (A) and (B). The conserved salt bridge residues Glu-Lys are shown as sticks with the salt bridge as dotted black lines and distorted R-spine depicted via a yellow surface with the gatekeeper residue as a red surface, with kinase domain of PAK5 colored as in (B), highlighting the accessible back-pocket (C). The displaced position of the conserved Glu-Lys salt bridge is shown as black dotted lines (navy-gray sticks) relative to TPX2-bound Aurora A in green (PDB: 1OL5) (D). The α C-helices of all known PAK5 molecules are shown, revealing the distortion seen with PAK5-Af17-bound PAK5 (E). The PAK5-Af17-bound PAK5 Arg487 (blue) is shown to swing distally away from the glycine-rich loop, aided by cation pi interactions with Tyr44 of Affimer variable region 1, distinct to the purine-bound conformation of Arg487 shown in cyan (PDB: 2F57), and the inactive Arg487 is shown in purple (PDB: 2F57, with the full side chain extrapolated in Coot) (F). The glycine rich loop of Affimer-bound PAK5 (orange) is shown overlaid with the inactive conformation (purple, PDB: 2F57, non-substrate-bound molecule) and the active conformation (marine, PDB: 2F57, substrate-bound molecule) and is stabilized by a novel hydrogen bond shown between Thr460 and Glu485 (G). The specificity of PAK5-Af17 toward PAK5 over the other group II PAKs is conferred by dynamic hydrogen bonds (dotted lines) between Pro77 of variable region 2 of PAK5-Af17, Glu37 of the Affimer backbone, and the PAK5-specific residue Arg653 (H), where mutation of the corresponding residues in PAK4 and PAK6 to arginine enhances PAK5-Af17 binding to these proteins as measured by phage ELISA (I) and immunoprecipitation of PAK5-Af17 by these proteins (J) (representative blot shown). Data are mean \pm SEM, n = 3 independent experiments for (I) and (J), one-way ANOVA with Dunnett's post hoc test. **p < 0.01.

understanding the mechanism of activation and abrogation of individual kinases, the development of more selective kinase inhibitors will advance and with it the landscape of cancer-specific therapeutics.

In conclusion, this study has presented a comprehensive high-content imaging assay for identifying all phases of the cell cycle, including G0 and apoptotic cells, used in conjunction with siRNA, followed up by generation of specific SBPs to identify PAK5 inhibitors and co-crystallization to understand the nature of the inhibition. We have shown the identification of specific cancer-type targets, in this case PAK5 (albeit only as specific as the number of counter-screens undertaken), together with determination of druggability and potential delineation of mechanism of action as seen by the locking of PAK5 in a previously unseen intermediate activation state. Applying this approach to other cancer types may yield new and exciting therapeutic targets.

Limitations of the study

This study has only briefly touched upon the biological impacts of PAK5 to generate a phenotypic fingerprint, and further work is required to determine the molecular details of the role of PAK5 in G1/S transition. The Affimers used in this study, while having clear biological effects similar to the siRNA, have not been fully characterized in terms of cellular stability and inhibitory effects beyond the 24-h expression time used here, although we have previously seen Affimers, for other targets, have cellular effects 48 h after transfection.¹¹ This study has not assessed the reversibility of PAK5 inhibition by PAK5-Af17. Additionally, while both X-ray crystallography and mutational analysis have demonstrated that PAK5-Af17 shows significant specificity for PAK5 over the other group II PAKs, it is possible that PAK5-Af17 has off-target effects on other kinases (including other PAKs) due to the high level of structural conservation between kinase active sites.⁸⁴

STAR★METHODS

Detailed methods are provided in the online version of this paper and include the following:

- **KEY RESOURCES TABLE**
- **RESOURCE AVAILABILITY**
 - Lead contact
 - Materials availability
 - Data and code availability
- **EXPERIMENTAL MODEL AND SUBJECT PARTICIPANT DETAILS**
 - Cell culture
- **METHOD DETAILS**
 - Mimosine synchronisation
 - siRNA transfections
 - Plasmid transfections
 - Immunofluorescent staining and imaging
 - Reverse transcription and quantitative PCR
 - Immunoprecipitation and immunoblotting
 - Protein production
 - Phage display and phage ELISA

- Kinase assay
- Crystallography
- Biacore surface plasmon resonance (SPR)
- **QUANTIFICATION AND STATISTICAL ANALYSIS**

SUPPLEMENTAL INFORMATION

Supplemental information can be found online at <https://doi.org/10.1016/j.celrep.2023.113184>.

ACKNOWLEDGMENTS

We thank Prof. Jonathan Chernoff for invaluable advice about PAK function and Dr. Matthew Adams for his technical assistance with siRNA screening. This work was supported by the Yorkshire Cancer Research grant number L377, Medical Research Council grant number MR/N020952/1, and Wellcome Trust grant number 102174/B/13/Z. We gratefully acknowledge funding from the MRC Mid-range equipment call for purchase of the Biacore 1K+ (MC_PC_MR/X013227/1). Graphical abstract was created with [BioRender.com](https://www.biorender.com) (2023).

AUTHOR CONTRIBUTIONS

H.L.M., M.A.K., and D.C.T. conceived the experimental plan. H.L.M., A.L.T., J.H., A.A.T., C.T., T.T., T.L.A., S.S., and I.W.M. conducted experimental work. All authors performed data analysis and critically reviewed and approved the manuscript.

DECLARATION OF INTERESTS

A.L.T. owns personal shares in Avacta Life Sciences. D.C.T. is a named inventor on the “artificial binding protein” patent, which is held by the University of Leeds and covers the Affimer reagents used in the study.

INCLUSION AND DIVERSITY

One or more of the authors of this paper self-identifies as an underrepresented ethnic minority in their field of research or within their geographical location. One or more of the authors of this paper self-identifies as a member of the LGBTQIA+ community.

Received: January 26, 2023
Revised: July 17, 2023
Accepted: September 13, 2023

REFERENCES

1. IARC (2020). *World Cancer Report 2020* (World Health Organisation).
2. Bellmunt, J., Ribas, A., Eres, N., Albanell, J., Almanza, C., Bermejo, B., Solé, L.A., and Baselga, J. (1997). Carboplatin-based versus cisplatin-based chemotherapy in the treatment of surgically incurable advanced bladder carcinoma. *Cancer* 80, 1966–1972. [https://doi.org/10.1002/\(sici\)1097-0142\(19971115\)80:10<1966::aid-cnrc14>3.0.co;2-w](https://doi.org/10.1002/(sici)1097-0142(19971115)80:10<1966::aid-cnrc14>3.0.co;2-w).
3. DiMasi, J.A., Grabowski, H.G., and Hansen, R.W. (2016). Innovation in the pharmaceutical industry: New estimates of R&D costs. *J. Health Econ.* 47, 20–33. <https://doi.org/10.1016/j.jhealeco.2016.01.012>.
4. Kana, O., and Brylinski, M. (2019). Elucidating the druggability of the human proteome with eFindSite. *J. Comput. Aided Mol. Des.* 33, 509–519. <https://doi.org/10.1007/s10822-019-00197-w>.
5. Škrlec, K., Štrukelj, B., and Berlec, A. (2015). Non-immunoglobulin scaffolds: a focus on their targets. *Trends Biotechnol.* 33, 408–418. <https://doi.org/10.1016/j.tibtech.2015.03.012>.
6. Deroo, S., Thiollay, S., Desmet, J., Baatz, F., Loverix, S., Vandenbroucke, K., Lorent, E., Henderikx, P., Lemmens, I., Alard, P., et al. (2016). Abstract

- 3850: First-in-class cell-penetrating proteins targeting Mcl-1 induce tumor cell apoptosis and inhibition of tumor growth *in vivo*. *Cancer Res.* 76, 3850. <https://doi.org/10.1158/1538-7445.AM2016-3850>.
7. Skrllec, K., Štrukelj, B., and Berlec, A. (2015). Non-immunoglobulin scaffolds: a focus on their targets. *Trends Biotechnol.* 33, 408–418. <https://doi.org/10.1016/j.tibtech.2015.03.012>.
 8. Tiede, C., Bedford, R., Heseltine, S.J., Smith, G., Wijetunga, I., Ross, R., AlQallaf, D., Roberts, A.P., Balls, A., Curd, A., et al. (2017). Affimer proteins are versatile and renewable affinity reagents. *Elife* 6, e24903. <https://doi.org/10.7554/eLife.24903>.
 9. Tiede, C., Tang, A.A.S., Deacon, S.E., Mandal, U., Nettleship, J.E., Owen, R.L., George, S.E., Harrison, D.J., Owens, R.J., Tomlinson, D.C., and McPherson, M.J. (2014). Adhiron: a stable and versatile peptide display scaffold for molecular recognition applications. *Protein Eng. Des. Sel.* 27, 145–155. <https://doi.org/10.1093/protein/gzu007>.
 10. Robinson, J.I., Baxter, E.W., Owen, R.L., Thomsen, M., Tomlinson, D.C., Waterhouse, M.P., Win, S.J., Nettleship, J.E., Tiede, C., Foster, R.J., et al. (2018). Affimer proteins inhibit immune complex binding to Fc γ 3bRIIIa with high specificity through competitive and allosteric modes of action. *Proc. Natl. Acad. Sci. USA* 115, E72–E81. <https://doi.org/10.1073/pnas.1707856115>.
 11. Haza, K.Z., Martin, H.L., Rao, A., Turner, A.L., Saunders, S.E., Petersen, B., Tiede, C., Tipping, K., Tang, A.A., Ajayi, M., et al. (2021). RAS-inhibiting biologics identify and probe druggable pockets including an SH- α 3 allosteric site. *Nat. Commun.* 12, 4045. <https://doi.org/10.1038/s41467-021-24316-0>.
 12. Johnson, D.G., and Walker, C.L. (1999). Cyclins and cell cycle checkpoints. *Annu. Rev. Pharmacol. Toxicol.* 39, 295–312. <https://doi.org/10.1146/annurev.pharmtox.39.1.295>.
 13. Rojas, A.M., Santamaria, A., Malik, R., Jensen, T.S., Körner, R., Morilla, I., de Juan, D., Krallinger, M., Hansen, D.A., Hoffmann, R., et al. (2012). Uncovering the molecular machinery of the human spindle—an integration of wet and dry systems biology. *PLoS One* 7, e31813. <https://doi.org/10.1371/journal.pone.0031813>.
 14. Malumbres, M. (2011). Physiological relevance of cell cycle kinases. *Physiol. Rev.* 91, 973–1007. <https://doi.org/10.1152/physrev.00025.2010>.
 15. Pagano, M., and Jackson, P.K. (2004). Wagging the dogma; tissue-specific cell cycle control in the mouse embryo. *Cell* 118, 535–538. <https://doi.org/10.1016/j.cell.2004.08.013>.
 16. Low, J., Chakravarty, A., Blosser, W., Dowless, M., Chalfant, C., Bragger, P., and Stancato, L. (2009). Phenotypic fingerprinting of small molecule cell cycle kinase inhibitors for drug discovery. *Curr. Chem. Genom.* 3, 13–21. <https://doi.org/10.2174/1875397300903010013>.
 17. Low, J., Huang, S., Blosser, W., Dowless, M., Burch, J., Neubauer, B., and Stancato, L. (2008). High-content imaging characterization of cell cycle therapeutics through in vitro and in vivo subpopulation analysis. *Mol. Cancer Therapeut.* 7, 2455–2463. <https://doi.org/10.1158/1535-7163.mct-08-0328>.
 18. Sutherland, J.J., Low, J., Blosser, W., Dowless, M., Engler, T.A., and Stancato, L.F. (2011). A robust high-content imaging approach for probing the mechanism of action and phenotypic outcomes of cell-cycle modulators. *Mol. Cancer Therapeut.* 10, 242–254. <https://doi.org/10.1158/1535-7163.mct-10-0720>.
 19. Mukherji, M., Bell, R., Supekova, L., Wang, Y., Orth, A.P., Batalov, S., Miraglia, L., Huesken, D., Lange, J., Martin, C., et al. (2006). Genome-wide functional analysis of human cell-cycle regulators. *Proc. Natl. Acad. Sci. USA* 103, 14819–14824. <https://doi.org/10.1073/pnas.0604320103>.
 20. Bedford, R., Tiede, C., Hughes, R., Curd, A., McPherson, M.J., Peckham, M., and Tomlinson, D.C. (2017). Alternative reagents to antibodies in imaging applications. *Biophys. Rev.* 9, 299–308. <https://doi.org/10.1007/s12551-017-0278-2>.
 21. Hughes, D.J., Tiede, C., Penswick, N., Tang, A.A.S., Trinh, C.H., Mandal, U., Zajac, K.Z., Gaule, T., Howell, G., Edwards, T.A., et al. (2017). Generation of specific inhibitors of SUMO-1- and SUMO-2/3-mediated protein-protein interactions using Affimer (Adhiron) technology. *Sci. Signal.* 10, eaaj2005. <https://doi.org/10.1126/scisignal.aaj2005>.
 22. Lopata, A., Hughes, R., Tiede, C., Heissler, S.M., Sellers, J.R., Knight, P.J., Tomlinson, D., and Peckham, M. (2018). Affimer proteins for F-actin: novel affinity reagents that label F-actin in live and fixed cells. *Sci. Rep.* 8, 6572. <https://doi.org/10.1038/s41598-018-24953-4>.
 23. Martin, H.L., Bedford, R., Heseltine, S.J., Tang, A.A., Haza, K.Z., Rao, A., McPherson, M.J., and Tomlinson, D.C. (2018). Non-immunoglobulin scaffold proteins: Precision tools for studying protein-protein interactions in cancer. *N. Biotech.* 45, 28–35. <https://doi.org/10.1016/j.nbt.2018.02.008>.
 24. Miles, J.A., Hobor, F., Trinh, C.H., Taylor, J., Tiede, C., Rowell, P.R., Jackson, B.R., Nadat, F.A., Ramsahye, P., Kyle, H.F., et al. (2021). Selective Affimers Recognise the BCL-2 Family Proteins BCL-x(L) and MCL-1 through Noncanonical Structural Motifs. *Chembiochem* 22, 232–240. <https://doi.org/10.1002/cbic.202000585>.
 25. Tang, A.A.S., Tiede, C., McPherson, M.J., and Tomlinson, D.C. (2021). Isolation of Artificial Binding Proteins (Affimer Reagents) for Use in Molecular and Cellular Biology. *Methods Mol. Biol.* 2247, 105–121. https://doi.org/10.1007/978-1-0716-1126-5_6.
 26. Manning, G., Whyte, D.B., Martinez, R., Hunter, T., and Sudarsanam, S. (2002). The protein kinase complement of the human genome. *Science (New York, N.Y.)* 298, 1912–1934. <https://doi.org/10.1126/science.1075762>.
 27. Barr, F.A., Silljé, H.H.W., and Nigg, E.A. (2004). Polo-like kinases and the orchestration of cell division. *Nat. Rev. Mol. Cell Biol.* 5, 429–440. <https://doi.org/10.1038/nrm1401>.
 28. Reinhardt, H.C., and Yaffe, M.B. (2013). Phospho-Ser/Thr-binding domains: navigating the cell cycle and DNA damage response. *Nat. Rev. Mol. Cell Biol.* 14, 563–580. <https://doi.org/10.1038/nrm3640>.
 29. Baldwin, A., Li, W., Grace, M., Pearlberg, J., Harlow, E., Münger, K., and Grueneberg, D.A. (2008). Kinase requirements in human cells: II. Genetic interaction screens identify kinase requirements following HPV16 E7 expression in cancer cells. *Proc. Natl. Acad. Sci. USA* 105, 16478–16483. <https://doi.org/10.1073/pnas.0806195105>.
 30. Bommi-Reddy, A., Almeciga, I., Sawyer, J., Geisen, C., Li, W., Harlow, E., Kaelin, W.G., Jr., and Grueneberg, D.A. (2008). Kinase requirements in human cells: III. Altered kinase requirements in VHL-/- cancer cells detected in a pilot synthetic lethal screen. *Proc. Natl. Acad. Sci. USA* 105, 16484–16489. <https://doi.org/10.1073/pnas.0806574105>.
 31. Moffat, J., Grueneberg, D.A., Yang, X., Kim, S.Y., Kloepper, A.M., Hinkle, G., Piquani, B., Eisenhaure, T.M., Luo, B., Grenier, J.K., et al. (2006). A lentiviral RNAi library for human and mouse genes applied to an arrayed viral high-content screen. *Cell* 124, 1283–1298. <https://doi.org/10.1016/j.cell.2006.01.040>.
 32. Cappella, P., and Gasparri, F. (2014). Highly multiplexed phenotypic imaging for cell proliferation studies. *J. Biomol. Screen* 19, 145–157. <https://doi.org/10.1177/1087057113495712>.
 33. Cappella, P., Gasparri, F., Pulici, M., and Moll, J. (2008). Cell proliferation method: click chemistry based on BrdU coupling for multiplex antibody staining. *Curr. Protoc. Cytom. Chapter 7*, Unit7.34. <https://doi.org/10.1002/0471142956.cy0734s45>.
 34. Scholzen, T., and Gerdes, J. (2000). The Ki-67 protein: from the known and the unknown. *J. Cell. Physiol.* 182, 311–322. [https://doi.org/10.1002/\(sici\)1097-4652\(200003\)182:3<311::aid-jcp1>3.0.co;2-9](https://doi.org/10.1002/(sici)1097-4652(200003)182:3<311::aid-jcp1>3.0.co;2-9).
 35. Spänkuch-Schmitt, B., Bereiter-Hahn, J., Kaufmann, M., and Strebhardt, K. (2002). Effect of RNA silencing of polo-like kinase-1 (PLK1) on apoptosis and spindle formation in human cancer cells. *J. Natl. Cancer Inst.* 94, 1863–1877.
 36. Kittler, R., Pelletier, L., Heninger, A.K., Slabicki, M., Theis, M., Miroslaw, L., Poser, I., Lawo, S., Grabner, H., Kozak, K., et al. (2007). Genome-scale RNAi profiling of human tissue culture cells. *Nat. Cell Biol.* 9, 1401–1412. <https://doi.org/10.1038/ncb1659>.

37. Lange, S.S., Takata, K.-i., and Wood, R.D. (2011). DNA polymerases and cancer. *Nat. Rev. Cancer* *11*, 96–110.
38. Nguyen, A., Rothman, D.M., Stehn, J., Imperiali, B., and Yaffe, M.B. (2004). Caged phosphopeptides reveal a temporal role for 14-3-3 in G1 arrest and S-phase checkpoint function. *Nat. Biotechnol.* *22*, 993–1000.
39. Birmingham, A., Selfors, L.M., Forster, T., Wrobel, D., Kennedy, C.J., Shanks, E., Santoyo-Lopez, J., Dunican, D.J., Long, A., Kelleher, D., et al. (2009). Statistical methods for analysis of high-throughput RNA interference screens. *Nat. Methods* *6*, 569–575. <https://doi.org/10.1038/nmeth.1351>.
40. Kumari, R., and Jat, P. (2021). Mechanisms of Cellular Senescence: Cell Cycle Arrest and Senescence Associated Secretory Phenotype. *Front. Cell Dev. Biol.* *9*, 645593. <https://doi.org/10.3389/fcell.2021.645593>.
41. Rodier, F., and Campisi, J. (2011). Four faces of cellular senescence. *J. Cell Biol.* *192*, 547–556. <https://doi.org/10.1083/jcb.201009094>.
42. Margadant, C., van Opstal, A., and Boonstra, J. (2007). Focal adhesion signaling and actin stress fibers are dispensable for progression through the ongoing cell cycle. *J. Cell Sci.* *120*, 66–76. <https://doi.org/10.1242/jcs.03301>.
43. Jones, M.C., Zha, J., and Humphries, M.J. (2019). Connections between the cell cycle, cell adhesion and the cytoskeleton. *Philos. Trans. R. Soc. Lond. B Biol. Sci.* *374*, 20180227. <https://doi.org/10.1098/rstb.2018.0227>.
44. Cotteret, S., Jaffer, Z.M., Beeser, A., and Chernoff, J. (2003). p21-Activated kinase 5 (Pak5) localizes to mitochondria and inhibits apoptosis by phosphorylating BAD. *Mol. Cell Biol.* *23*, 5526–5539.
45. Pandey, A., Dan, I., Kristiansen, T.Z., Watanabe, N.M., Voldby, J., Kajikawa, E., Khosravi-Far, R., Blagoev, B., and Mann, M. (2002). Cloning and characterization of PAK5, a novel member of mammalian p21-activated kinase-II subfamily that is predominantly expressed in brain. *Oncogene* *21*, 3939–3948.
46. Seibel, N.M., Eljouni, J., Nalaskowski, M.M., and Hampe, W. (2007). Nuclear localization of enhanced green fluorescent protein homomultimers. *Anal. Biochem.* *368*, 95–99. <https://doi.org/10.1016/j.ab.2007.05.025>.
47. Umezawa, K., and Kii, I. (2021). Druggable Transient Pockets in Protein Kinases. *Molecules* *26*, 651.
48. Eswaran, J., Lee, W.H., Debreczeni, J.E., Filippakopoulos, P., Turnbull, A., Fedorov, O., Deacon, S.W., Peterson, J.R., and Knapp, S. (2007). Crystal Structures of the p21-activated kinases PAK4, PAK5, and PAK6 reveal catalytic domain plasticity of active group II PAKs. *Structure* *15*, 201–213.
49. Modi, V., and Dunbrack, R.L. (2019). Defining a new nomenclature for the structures of active and inactive kinases. *Proc. Natl. Acad. Sci. USA* *116*, 6818–6827. <https://doi.org/10.1073/pnas.1814279116>.
50. Roskoski, R., Jr. (2016). Classification of small molecule protein kinase inhibitors based upon the structures of their drug-enzyme complexes. *Pharmacol. Res.* *103*, 26–48.
51. Zhang, E.Y., Ha, B.H., and Boggon, T.J. (2018). PAK4 crystal structures suggest unusual kinase conformational movements. *Biochim. Biophys. Acta, Proteins Proteomics* *1866*, 356–365.
52. Burgess, S.G., Oleksy, A., Cavazza, T., Richards, M.W., Vernos, I., Matthews, D., and Bayliss, R. (2016). Allosteric inhibition of Aurora-A kinase by a synthetic vNAR domain. *Open Biol.* *6*, 160089.
53. Cohen, P., Cross, D., and Jänne, P.A. (2021). Kinase drug discovery 20 years after imatinib: progress and future directions. *Nat. Rev. Drug Discov.* *20*, 551–569. <https://doi.org/10.1038/s41573-021-00195-4>.
54. Aguirre-Ghiso, J.A. (2007). Models, mechanisms and clinical evidence for cancer dormancy. *Nat. Rev. Cancer* *7*, 834–846. <https://doi.org/10.1038/nrc2256>.
55. Lera, R.F., and Burkard, M.E. (2012). High mitotic activity of Polo-like kinase 1 is required for chromosome segregation and genomic integrity in human epithelial cells. *J. Biol. Chem.* *287*, 42812–42825. <https://doi.org/10.1074/jbc.M112.412544>.
56. Kellogg, D.R. (2003). Wee1-dependent mechanisms required for coordination of cell growth and cell division. *J. Cell Sci.* *116*, 4883–4890. <https://doi.org/10.1242/jcs.00908>.
57. Nikonova, A.S., Astsaturov, I., Serebriiskii, I.G., Dunbrack, R.L., Jr., and Golemis, E.A. (2013). Aurora A kinase (AURKA) in normal and pathological cell division. *Cell. Mol. Life Sci.* *70*, 661–687. <https://doi.org/10.1007/s00018-012-1073-7>.
58. Bartek, J., and Lukas, J. (2003). Chk1 and Chk2 kinases in checkpoint control and cancer. *Cancer Cell* *3*, 421–429. [https://doi.org/10.1016/S1535-6108\(03\)00110-7](https://doi.org/10.1016/S1535-6108(03)00110-7).
59. Gu, J., Li, K., Li, M., Wu, X., Zhang, L., Ding, Q., Wu, W., Yang, J., Mu, J., Wen, H., et al. (2013). A role for p21-activated kinase 7 in the development of gastric cancer. *FEBS J.* *280*, 46–55.
60. Gu, Y.F., and Kong, L.T. (2021). Inhibiting p21-activated kinase (PAK7) enhances radiosensitivity in hepatocellular carcinoma. *Hum. Exp. Toxicol.* *40*, 2202–2214. <https://doi.org/10.1177/09603271211027948>.
61. Han, Z.X., Wang, X.X., Zhang, S.N., Wu, J.X., Qian, H.y., Wen, Y.y., Tian, H., Pei, D.S., and Zheng, J.N. (2014). Downregulation of PAK5 inhibits glioma cell migration and invasion potentially through the PAK5-Egr1-MMP2 signaling pathway. *Brain Tumor Pathol.* *31*, 234–241.
62. Huang, S., Zhu, Y., Wang, C., Li, X., Cui, X., Tu, S., You, L., Fu, J., Chen, Z., Hu, W., and Gong, W. (2020). PAK5 facilitates the proliferation, invasion and migration in colorectal cancer cells. *Cancer Med.* *9*, 4777–4790. <https://doi.org/10.1002/cam4.3084>.
63. Huo, F.-C., Pan, Y.-J., Li, T.-T., Mou, J., and Pei, D.-S. (2019). PAK5 promotes the migration and invasion of cervical cancer cells by phosphorylating SATB1. *Cell Death Differ.* *26*, 994–1006. <https://doi.org/10.1038/s41418-018-0178-4>.
64. Li, D., Pan, Y., Huang, Y., Zhang, P., and Fang, X. (2018). PAK5 Induces EMT and Promotes Cell Migration and Invasion by Activating the PI3K/AKT Pathway in Ovarian Cancer. *Anal. Cell Pathol.* *2018*, 8073124. <https://doi.org/10.1155/2018/8073124>.
65. Zhang, Y.-C., Huo, F.-C., Wei, L.-L., Gong, C.-C., Pan, Y.-J., Mou, J., and Pei, D.-S. (2017). PAK5-mediated phosphorylation and nuclear translocation of NF- κ B-p65 promotes breast cancer cell proliferation in vitro and in vivo. *J. Exp. Clin. Cancer Res.* *36*, 146. <https://doi.org/10.1186/s13046-017-0610-5>.
66. Ismail, A.F., Oskay Halacli, S., Babteen, N., De Piano, M., Martin, T.A., Jiang, W.G., Khan, M.S., Dasgupta, P., and Wells, C.M. (2017). PAK5 mediates cell adhesion integrity via interaction with E-cadherin in bladder cancer cells. *Biochem. J.* *474*, 1333–1346.
67. Fang, Z.-p., Jiang, B.-g., Gu, X.-f., Zhao, B., Ge, R.-l., and Zhang, F.-b. (2014). P21-activated kinase 5 plays essential roles in the proliferation and tumorigenicity of human hepatocellular carcinoma. *Acta Pharmacol. Sin.* *35*, 82–88. <https://doi.org/10.1038/aps.2013.31>.
68. Eray, A., and Erkek-Özhan, S. (2021). Classification of bladder cancer cell lines according to regulon activity. *Turk. J. Biol.* *45*, 656–666.
69. Xing, Y., Li, Y., Hu, B., Han, F., Zhao, X., Zhang, H., Li, Y., Li, D., Li, J., Jin, F., and Li, F. (2021). PAK5-mediated AIF phosphorylation inhibits its nuclear translocation and promotes breast cancer tumorigenesis. *Int. J. Biol. Sci.* *17*, 1315–1327.
70. Jones, M.C., Askari, J.A., Humphries, J.D., and Humphries, M.J. (2018). Cell adhesion is regulated by CDK1 during the cell cycle. *J. Cell Biol.* *217*, 3203–3218.
71. Jones, M.C., Zha, J., and Humphries, M.J. (2019). Connections between the cell cycle, cell adhesion and the cytoskeleton. *Philos. Trans. R. Soc. Lond. B Biol. Sci.* *374*, 20180227. <https://doi.org/10.1098/rstb.2018.0227>.
72. Eby, J.J., Holly Sp Fau - van Drogen, F., van Drogen F Fau - Grishin, A.V., Grishin Av Fau - Peter, M., Peter M, Fau - Drubin, D.G., Drubin Dg Fau - Blumer, K.J., and Blumer, K.J. Actin cytoskeleton organization regulated by the PAK family of protein kinases.
73. Tabanifar, B., Zhao, Z., and Manser, E. PAK5 Is Auto-Activated by a Central Domain that Promotes Kinase Oligomerization.

74. Rennefahrt, U.E.E., Deacon, S.W., Parker, S.A., Devarajan, K., Beeser, A., Chernoff, J., Knapp, S., Turk, B.E., and Peterson, J.R. (2007). Specificity Profiling of Pak Kinases Allows Identification of Novel Phosphorylation Sites. *J. Biol. Chem.* **282**, 15667–15678. <https://doi.org/10.1074/jbc.M700253200>.
75. Yi, C., Maksimoska, J., Marmorstein, R., and Kissil, J.L. (2010). Development of small-molecule inhibitors of the group I p21-activated kinases, emerging therapeutic targets in cancer. *Biochem. Pharmacol.* **80**, 683–689. <https://doi.org/10.1016/j.bcp.2010.03.012>.
76. Murray, B.W., Guo, C., Piraino, J., Westwick, J.K., Zhang, C., Lamerdin, J., Dagostino, E., Knighton, D., Loi, C.-M., Zager, M., et al. (2010). Small-molecule p21-activated kinase inhibitor PF-3758309 is a potent inhibitor of oncogenic signaling and tumor growth. *Proc. Natl. Acad. Sci. USA* **107**, 9446–9451.
77. Trials, C. <https://clinicaltrials.gov/ct2/show/NCT00932126>.
78. Deacon, S.W., Beeser, A., Fukui, J.A., Rennefahrt, U.E.E., Myers, C., Chernoff, J., and Peterson, J.R. (2008). An isoform-selective, small-molecule inhibitor targets the autoregulatory mechanism of p21-activated kinase. *Chem. Biol.* **15**, 322–331.
79. Staben, S.T., Feng, J.A., Lyle, K., Belvin, M., Boggs, J., Burch, J.D., Chua, C.-c., Cui, H., DiPasquale, A.G., Friedman, L.S., et al. (2014). Back pocket flexibility provides group II p21-activated kinase (PAK) selectivity for type I 1/2 kinase inhibitors. *J. Med. Chem.* **57**, 1033–1045.
80. Karpov, A.S., Amiri, P., Bellamacina, C., Bellance, M.H., Breitenstein, W., Daniel, D., Denay, R., Fabbro, D., Fernandez, C., Galuba, I., et al. (2015). Optimization of a Dibenzodiazepine Hit to a Potent and Selective Allosteric PAK1 Inhibitor. *ACS Med. Chem. Lett.* **6**, 776–781.
81. Coffey, G., DeGuzman, F., Inagaki, M., Pak, Y., Delaney, S.M., Ives, D., Betz, A., Jia, Z.J., Pandey, A., Baker, D., et al. (2012). Specific Inhibition of Spleen Tyrosine Kinase Suppresses Leukocyte Immune Function and Inflammation in Animal Models of Rheumatoid Arthritis. *J. Pharmacol. Exp. Therapeut.* **340**, 350–359. <https://doi.org/10.1124/jpet.111.188441>.
82. Baskaran, Y., Ang, K.C., Anekal, P.V., Chan, W.L., Grimes, J.M., Manser, E., and Robinson, R.C. (2015). An in cellulo-derived structure of PAK4 in complex with its inhibitor Inka1. *Nat. Commun.* **6**, 8681. <https://doi.org/10.1038/ncomms9681>.
83. Richards, M.W., Burgess, S.G., Poon, E., Carstensen, A., Eilers, M., Chesler, L., and Bayliss, R. (2016). Structural basis of N-Myc binding by Aurora-A and its destabilization by kinase inhibitors. *Proc. Natl. Acad. Sci. USA* **113**, 13726–13731.
84. Modi, V., and Dunbrack, R.L. (2019). A Structurally-Validated Multiple Sequence Alignment of 497 Human Protein Kinase Domains. *Sci. Rep.* **9**, 19790. <https://doi.org/10.1038/s41598-019-56499-4>.
85. Askham, J.M., Platt, F., Chambers, P.A., Snowden, H., Taylor, C.F., and Knowles, M.A. (2010). AKT1 mutations in bladder cancer: identification of a novel oncogenic mutation that can co-operate with E17K. *Oncogene* **29**, 150–155.
86. Adams, M., Cookson, V.J., Higgins, J., Martin, H.L., Tomlinson, D.C., Bond, J., Morrison, E.E., and Bell, S.M. (2014). A High-Throughput Assay to Identify Modifiers of Premature Chromosome Condensation. *J. Biomol. Screen* **19**, 176–183. <https://doi.org/10.1177/1087057113495443>.
87. Nolan, T., Hands, R.E., and Bustin, S.A. (2006). Quantification of mRNA using real-time RT-PCR. *Nat. Protoc.* **1**, 1559–1582. <https://doi.org/10.1038/nprot.2006.236>.
88. Winter, G., Lobley, C.M.C., and Prince, S.M. (2013). Decision making in xia2. *Acta Crystallogr. D* **69**, 1260–1273. <https://doi.org/10.1107/S0907444913015308>.
89. Harada, H., Becknell, B., Wilm, M., Mann, M., Huang, L.J., Taylor, S.S., Scott, J.D., and Korsmeyer, S.J. (1999). Phosphorylation and inactivation of BAD by mitochondria-anchored protein kinase A. *Mol. Cell* **3**, 413–422.
90. McCoy, A.J., Grosse-Kunstleve, R.W., Adams, P.D., Winn, M.D., Storoni, L.C., and Read, R.J. (2007). Phaser crystallographic software. *J. Appl. Crystallogr.* **40** (Pt 4), 658–674.
91. Murshudov, G.N., Vagin, A.A., and Dodson, E.J. (1997). Refinement of macromolecular structures by the maximum-likelihood method. *Acta Crystallogr. D Biol. Crystallogr.* **53** (Pt 3), 240–255.
92. Emsley, P., and Cowtan, K. (2004). Coot: model-building tools for molecular graphics. *Acta Crystallogr. D Biol. Crystallogr.* **60** (Pt 12 Pt 1), 2126–2132.

STAR★METHODS

KEY RESOURCES TABLE

REAGENT or RESOURCE	SOURCE	IDENTIFIER
Antibodies		
Mouse anti-Histone H3	Abcam	Cat# ab14955; RRID:AB_443110
Rabbit anti-Ki67	Abcam	Cat# ab16667; RRID:AB_302459
Goat anti-mouse Alexa Fluor 568	Invitrogen	Cat#A-11004; RRID:AB_2534072
Goat anti-rabbit Alexa Fluor 633	Invitrogen	Cat#A-21070; RRID:AB_2535731
Rabbit anti-cyclin D1	Abcam	Cat# ab134175; RRID:AB_2750906
Rat anti- α -tubulin	Bio-Rad	Cat# MCA78G; RRID:AB_325005
Mouse anti-PAK5 (PAK7)	Novus Biologicals	Cat#MAB4696 RRID:N/A
Rabbit anti-p21	Abcam	Cat# ab109520; RRID:AB_10860537
Rabbit anti-phosphorylated BAD	Abcam	Cat# ab129192; RRID:AB_11142421
Mouse anti-turboGFP	Origene	Cat# TA150041; RRID:AB_2622256
Mouse anti-6xHisTag	Abcam	Cat# ab18184; RRID:AB_444306
Rabbit anti-6xHisTag-HRP	Abcam	Cat#ab1187; RRID:AB_298652
Goat- <i>anti</i> -rabbit HRP	Abcam	Cat# ab97051; RRID:AB_10679369
Goat anti-mouse HRP	Abcam	Cat# ab97040; RRID:AB_10698223
Goat anti-rat HRP	Abcam	Cat# ab97057; RRID:AB_10680316
Anti-Fd-Bacteriophage-HRP	Seramun Diagnostica GmbH	Cat# A-020-1-HRP RRID:N/A
Bacterial and virus strains		
BL21 Star TM (DE3)	Invitrogen	Cat# C601003
XL1-Blue Super-competent	Aglient	Cat#200249
ER2738	Lucigen	Cat#60522-1
Chemicals, peptides, and recombinant proteins		
L-mimosine	SigmaAldrich	Cat#M0253 CAS: 500-44-7
Critical commercial assays		
Click-iT [®] EdU Alexa Fluor [®] 488 HCS Assay *2-plate size*	Invitrogen	Cat#C10350
Click-iT [®] EdU Alexa Fluor [®] 647 HCS Assay *2-plate size*	Invitrogen	Cat#C10356
RNeasy Mini Kit	Qiagen	Cat#74106
qPCR Gene expression assays PLK1	Solaris	Cat# AX-017199
qPCR Gene expression assays PSMB1	Solaris	Cat# AX-011361
qPCR Gene expression assays POLA1	Solaris	Cat# AX-020856
qPCR Gene expression assays CCNE1	Solaris	Cat# AX-003213
qPCR Gene expression assays EEF1A1	Solaris	Cat# AX-017201
Deposited data		
PAK5:PAK5-Af17 structure	This Paper	PDB:8C12
Experimental models: Cell lines		
Human U-2 OS osteosarcoma cells	ATCC	Cat# HTB-96; RRID:CVCL_0042
Human 5637 urothelial carcinoma cells	ATCC	Cat# HTB-9; RRID:CVCL_0126
SD urothelial carcinoma cells	ATCC	RRID:CVCL_W902
LUC3 urothelial carcinoma cells	(Askham JM et al.) ⁸⁵	RRID:CVCL_W894

(Continued on next page)

REAGENT or RESOURCE	SOURCE	IDENTIFIER
Continued		
Oligonucleotides		
Human Protein Kinase siRNA library (siGenome)	Dharmacon	Cat#G003505
NT siRNA (siGenome)	Dharmacon	Cat# D-001206-14-20
PLK1 siRNA (siGenome)	Dharmacon	Cat# M-003290-01-0005
<i>PSMB1</i> siRNA (siGenome)	Dharmacon	Cat# M-011361-00-0005
<i>POLA1</i> siRNA (siGenome)	Dharmacon	Cat# M-020856-01-0005
<i>CCNE1</i> siRNA (siGenome)	Dharmacon	Cat# M-003213-02-0005
<i>PAK5</i> siRNA (siGenome)	Dharmacon	Cat# M-003973-02-0005
<i>PAK5</i> siRNA (ON TARGETplus)	Dharmacon	Cat# L-003973-00-0005
NT (ON TARGETplus)	Dharmacon	Cat# D-001810-10-20
<i>PLK1</i> (ON TARGETplus)	Dharmacon	Cat# L-003290-00-0005
Primers for used subcloning	See Table S4	
Recombinant DNA		
PAK5-GFP	Origene	Cat# RG205255
PAK5-Af-GFP	This Paper	N/A
Control-Af-GFP	This Paper	N/A
Af-His	This Paper	N/A
pcDNA3.1 PAK-5-FLAG	Genscript	N/A
PAK5-His	This Paper	N/A
PAK4-GST	Nicola Burgess-Brown	Addgene Cat#39137; RRID:Addgene_39137
PAK6-His	Nicola Burgess-Brown	Addgene Cat#38827; RRID:Addgene_38827
pGEX4T-1 BAD S136A (104–141)	Harada et al. ⁸⁴	Addgene Cat#8801; RRID:Addgene_8801
Software and algorithms		
Columbus v2.7.1	PerkinElmer	https://www.perkinelmer.com/product/image-data-storage-and-analysis-system-columbus
CellReporterXpress v2.8.2	Molecular Devices	https://www.moleculardevices.com/products/cellular-imaging-systems/acquisition-and-analysis-software/cellreporterxpress
MetaXpress	Molecular Devices	https://www.moleculardevices.com/products/cellular-imaging-systems/acquisition-and-analysis-software/metaxpress
GraphPad Prism v9.02	GraphPad Software	https://www.graphpad.com/features
Excel 2016	Microsoft	https://www.microsoft.com/en/microsoft-365/excel

RESOURCE AVAILABILITY

Lead contact

Further information and requests for resources and reagents should be directed to and will be fulfilled by the lead contact, Darren Tomlinson (d.c.tomlinson@leeds.ac.uk).

Materials availability

All unique/stable reagents generated in this study are available from the [lead contact](#) with a completed materials transfer agreement.

Data and code availability

- PAK5:PAK5-Af17 crystallisation data have been deposited at RCSB Protein DataBank (RCSB PDB) and are publicly available as of the date of publication. Accession numbers are listed in the [key resources table](#).
- All original code is available in this paper's supplemental information.
- Any additional information required to reanalyze the data reported in this paper is available from the [lead contact](#) upon request.

EXPERIMENTAL MODEL AND SUBJECT PARTICIPANT DETAILS

Cell culture

Human U-2 OS osteosarcoma cells (female; ATCC, VA) were maintained in Dulbecco's Modified Eagle's Medium (DMEM; PAA Laboratories GmbH, Pasching, Austria) supplemented with 10% fetal bovine serum (FBS; PAA) and 100U/mL penicillin-streptomycin (PAA) at 37°C and 5% CO₂. Human 5637 (male) and SD urothelial carcinoma cells (sex unspecified at primary collection; ATCC) were maintained in RPMI supplemented with 10% fetal bovine serum (FBS; PAA) and 100U/mL penicillin-streptomycin (PAA). LUC3 urothelial carcinoma cells were established in Leeds from a high grade muscle-invasive bladder cancer (sex unspecified at primary collection)⁸⁵ and maintained in Hams F12 medium supplemented with 1% FBS, 1% insulin-transferrin-selenium (Gibco, Paisley, UK), 1 μg/mL hydrocortisone (SigmaAldrich, Gillingham, UK), 1% non-essential amino acids (Gibco), 1% L-glutamine (Gibco) and 30 ng/mL cholera toxin (SigmaAldrich) at 37°C and 5% CO₂. The identity of all cell lines used was confirmed by Short Tandem Repeat (STR) profiling.

METHOD DETAILS

Mimosine synchronisation

U-2 OS cells were plated at 4000 cells/well in 96 well plates (Viewpoint, PerkinElmer, Waltham, MA) and treated with 500 μM L-mimosine (SigmaAldrich) 24 h later. L-mimosine was removed after a further 24 h and cells rinsed and incubated with 10 μM 5-ethynyl-2'-deoxyuridine (EdU, Invitrogen) for 30 min at 37 °C at designated time-intervals before phosphate buffered saline (PBS) rinsing and fixation in 4% paraformaldehyde (SigmaAldrich) for 15 min. Cells were then stained and imaged as described below.

siRNA transfections

Dharmacon siGENOME SMARTpool reagents (Human Protein Kinase library - G003505) were used for primary screening and were reconstituted as previously described.⁸⁶ Assay controls were non-targeting (NT) siRNA (D-001206-13), *PLK1* (M-003290), *PSMB1* (M-011361), *POLA1* (M-020856) and *CCNE1* (M-003213). Reverse transfections in 96 well plates were as previously described⁸⁶ using 2.5 μL of 2 μM siRNA (final concentration of 50 nM), 0.1 μL Lipofectamine RNAiMAX (Invitrogen), 17.5 μL Opti-MEM-1 (Invitrogen) and 80 μL of a 5 × 10⁴ cells/mL suspension in antibiotic-free media per well for U-2 OS cells or 7.5 × 10⁴ cells/mL suspensions for 5637, SD and LUC3 cells. For RNA extractions 24 well plates were used and 6 well plates for protein extractions reagent volumes increased to give 500 μL and 2 mL total well volume respectively. For validation assays Dharmacon ONTARGETplus SMARTpool reagents were used as above for siGENOME reagents.

Plasmid transfections

For transfection with PAK5-GFP (Origene, Rockville, MD) 5367 cells were plated at 5 × 10⁴ cells/mL in T75 flasks before transfection 72hr later with 25 μg plasmid DNA and 25 μL Lipofectamine 2000 (Invitrogen) as per manufacturer's instructions. Cells were harvested 24 h later. For transfections with PAK5-Af-GFP or Control-Af-GFP, 5637 cells were plated at 2.5 × 10⁴ cells/ml in 96 well Viewplates or 6 well plates, 72 h later transfected with 1 μg/mL plasmid using Lipofectamine 2000 at 2 μL/mL and fixed or harvested 24 h later as described below.

Immunofluorescent staining and imaging

Immunofluorescent staining of cell-cycle assay plates was carried out as follows. Media was discarded and cells incubated with 10 μM EdU as described for mimosine synchronisation. Following fixation with 4% paraformaldehyde, cells were rinsed twice with PBS and permeabilised with 0.1% Triton X-100 (VWR, Lutterworth, UK) in PBS for 15 min, before incubation with AlexaFluorTM 488 or 647 azide (Alexa Fluor 488/647 5-Carboxamido-(6-Azido)hexanyl), Bis(Triethylammonium Salt), Invitrogen) and Click-IT cell reaction buffer (Invitrogen) as described by the manufacturer for 30 min. Cells were rinsed in PBS and blocked in 1% milk (Marvel, Premier Foods, St Albans, UK) for 5 min before the addition of mouse anti-Histone H3 (phospho S10, 1:5000; Abcam ab14955; Cambridge, UK), rabbit anti-Ki67 (1:200; Abcam ab16667) diluted in 1% milk for 1 h in the dark, at room temperature. Following PBS rinses, cells were incubated at room temperature for 1 h in the dark, with 1% milk containing goat anti-mouse AlexaFluorTM 568 (1:3000; Molecular Probes, Eugene, OR), goat anti-rabbit AlexaFluorTM 633 (1:1000; Molecular Probes) and 1 μg/mL DAPI (Molecular Probes). Following a final set of PBS washes, plates were scanned and images collected with an Operetta HTS imaging system (PerkinElmer) at 20× magnification with 11 fields of view (510 × 675 μm)/well. Images were analyzed in Columbus 2.2 (PerkinElmer) with a custom protocol (Table S1) and wells containing artifacts were removed from the dataset (n = 6).

For PAK5 morphology analysis, wheatgerm agglutinin AlexaFluorTM 633 was added for 10 min prior to Triton X- permeabilisation, followed by PBS rinse and incubation with DAPI for 1 h at room temperature in 1% milk before rinsing in PBS and imaged on the Operetta HTS and analyzed with Columbus 2.2. F-actin was stained with Alexa Fluor 488/647 phalloidin (1:500, Molecular Probes) in conjunction with DAPI staining imaged on the Operetta HTS and analyzed with Columbus 2.2. Later experiments were imaged using ImageXpress Pico (Molecular Devices) and analyzed in MetaXpress v 6.7 (Molecular Devices).

Reverse transcription and quantitative PCR

RNA was extracted at 72 and 96 h post transfection using a RNeasy kit (Qiagen, Manchester, UK), as per the manufacturer's instructions, and quantified with a Qubit 2.0 (Invitrogen). cDNA was synthesised from 100 ng RNA using Superscript II (Invitrogen) and oligo dT (Ambion, Austin, TX) as per manufacturer's instructions. Quantitative PCR was performed using Solaris qPCR Gene expression assays (PLK1 – AX-017199, PSMB1 – AX-011361, POLA1 – AX-020856, CCNE1 - AX-003213 and EEF1A1 – AX-017201; ThermoFisher, Waltham, MA) with Applied Biosystems 7500 Real-Time PCR machine as per manufacturer's instructions. Data were analyzed using the ddCT method.⁸⁷

Immunoprecipitation and immunoblotting

Cells were rinsed in PBS and lysed in 50 μ L RIPA buffer (ThermoFisher)/9cm² supplemented with HaltTM EDTA free protease inhibitor cocktail (Pierce) and phosphatase inhibitor 2 (SigmaAldrich) followed by centrifugation at 10,000 xg for 15 min at 4°C. Protein concentrations were measured by BCA assay, as per manufacturer's instructions (ThermoFisher).

For PAK5 immunoprecipitation from lysates of cells transfected with PAK5-GFP, His-Tag Dynabeads (ThermoFisher) and the Kingfisher Flex (ThermoFisher) were utilised. Dynabeads were incubated with 50 μ g PAK5 or control Affimers in 1x blocking buffer (SigmaAldrich) in wash buffer (100 mM Sodium-phosphate, pH 8.0, 600 mM NaCl, 0.02% Tween 20) for 10 min, and rinsed with wash buffer. Beads were then incubated with 1 mg lysate for⁸⁸ mins at room temperature. Following three washes, proteins were eluted by incubation in His elution buffer (300 mM Imidazole, 50 mM Sodium phosphate, pH 8.0, 300 mM NaCl, 0.01% Tween 20) for 10 min. Immunoprecipitants were heated in 4x LBS buffer containing 50 mM DTT and run on a 12% SDS-PAGE gel.

For immunoprecipitation of purified Group II PAK proteins with PAK5-Af17 or control Affimers MyOne Streptavidin T1 Dynabeads (ThermoFisher) and the Kingfisher Flex were utilised. Dynabeads were incubated with 2x blocking buffer in PBS +0.003% CHAPS overnight at room temperature, blocking buffer was removed and the beads were incubated with 5 μ g of biotinylated PAK proteins in 2x blocking buffer in PBS-T for an hour with rotation at room temperature. The beads were washed three times with PBST and incubated with 0.5 μ g of PAK5-Af17 or control Affimer for 1 h. Following four PBS-T washes, proteins were then eluted in SDS-PAGE sample buffer (200 mM Tris-HCl, 8% SDS, 20% glycerol, 20% mercaptoethanol, 0.1% (w/v) bromophenol blue, pH 7) and 2.5 μ L of these elutions run on a 15% SDS-PAGE gel.

For immunoblotting 20–50 μ g of lysates were heated with 4x LBS containing 50 mM DTT for 10 min at 70°C, loaded onto Tris-HEPES gels and run at 120 V before transfer to nitrocellulose membrane using the BioRad Transblot Turbo. Membranes were then blocked in 5% milk in TBS-T before overnight incubation at 4°C with rabbit anti-cyclin D1 (1:10,000, Abcam ab134175), rat anti- α -tubulin (1:3000, BioRad, Hercules, CA, MCA78G), mouse anti-PAK5 (1:1000 Novus Biologicals, Abingdon, UK 444703), rabbit anti-p21 (1:10,000, Abcam ab109520), rabbit anti-phosphorylated BAD (1:20,000 Abcam, ab129192), mouse anti-turboGFP (1:5000, Origene, Rockville, MD, TA150041), mouse anti-6xHisTag (1:50,000 or 1:100,000, Abcam, ab18184), or rabbit anti-6xHisTag-HRP (1:10,000 for 1 h at room temperature, Abcam, ab1187). Membranes were rinsed three times with TBS-T before 1 h incubation at room temperature with goat-*anti*-rabbit HRP (Abcam, ab97051), goat anti-mouse HRP (Abcam, ab97040) or goat anti-rat HRP (Abcam, ab97057) if required, followed by three more TBS-T rinses, and development using Immunoblot Forte Western HRP (Millipore), according to the manufacturer's instructions. Blots were imaged using an AmershamTM Imager 600 (GE Healthcare, Chicago, IL). Images were analyzed with ImageQuant TL v8.1.0.0 (GE Healthcare).

Protein production

PAK5 kinase domain (amino acids 426 to 719) was subcloned from pcDNA3.1 PAK-5-FLAG (Genscript, Oxford UK) into pET11a. PAK4-GST (Addgene plasmid #39137) and PAK6-His (Addgene plasmid #38827) were gifts from Nicola Burgess-Brown, and pGEX4T-1 BAD S136A (104–141) was a gift from Stanley Korsmeyer (Addgene plasmid # 8801⁸⁹). Protein, including Affimer, production was as previously described in BL21 STARTM (DE3) *E. coli* 8,9. Briefly, a single colony was used to inoculate a 7 mL overnight culture of LB media supplemented with 100 μ g/mL carbenicillin (PAK4, PAK5, BAD and Affimers) or 50 μ g/mL kanamycin (PAK6). Then, 400 mL LB media plus antibiotic was inoculated with 5 mL of the overnight culture and grown at 37°C and 230 rpm to an OD₆₀₀ between 0.6 and 0.8. Protein production was induced by addition of IPTG 0.1 mM and incubated for a further 20–22 h, at 25°C and 150 rpm before harvesting. His-tagged proteins were lysed in 1 mL lysis buffer (50 mM NaH₂PO₄, 300 mM NaCl, 30 mM Imidazole, 10% Glycerol, 1% Triton X-100, pH 7.4) supplemented with 0.1 mg/mL lysozyme, Halt protease inhibitor cocktail and 10 U/ml benzonase nuclease (Millipore, Burlington, MA). The lysate was then incubated with 800 μ L of washed NiNTA slurry (Abcam) for 2 h, washed (50 mM NaH₂PO₄, 500 mM NaCl, 20 mM Imidazole, pH 7.4) and eluted in elution buffer (50 mM NaH₂PO₄, 500 mM NaCl, 300 mM Imidazole, 20% glycerol, pH 7.4). GST-tagged proteins were lysed in GST-lysis buffer (125 mM Tris-HCl, 150 mM NaCl, 1 mM DTT, 1 mM EDTA, 1% Triton X-, pH 7.4) supplemented with 1 mg/mL lysozyme, Halt protease inhibitor cocktail and 3 U/ml benzonase nuclease. The lysate was then incubated with 1 mL of washed SuperGlu Agarose Affinity resin (Generon, Slough, UK) for 2 h, washed (125 mM Tris-HCl, 150 mM NaCl, 1 mM DTT, 1 mM EDTA, pH 7.4) and eluted in 1 mL GST-elution buffer (125 mM Tris-HCl, 150 mM NaCl, 1 mM DTT, 1% Triton X-, 50 mM reduced glutathione, pH 7.4). BAP-tagged PAK proteins were produced by subcloning the PAK kinase domains into pET11 with a C-terminal BAP-tag preceding the His-tag. The mutations of PAK4 and PAK6 were generated using site directed mutagenesis. Proteins were expressed in BL21 STARTM (DE3) *E. coli* containing the pBirAcm plasmid in the presence of 10 μ g/mL chloramphenicol and 100 μ g/mL carbenicillin at 25°C and 200 rpm to an OD₆₀₀ between 0.6 and 0.8. Protein production was induced by addition of IPTG 0.1 mM and 50 μ M biotin then incubated for a further

20–22 h, at 25°C and 150 rpm before harvesting. Purification was as for His-tagged proteins using HEPES buffers (lysis and wash buffer; 20 mM HEPES, 150 mM NaCl, 10 mM MgCl₂, 20 mM imidazole and 0.5% glycerol, pH 7.5; Elution buffer was as lysis and wash buffer, but with 300mM imidazole). Affimer protein production was as previously described^{8,9}.

Phage display and phage ELISA

Target biotinylation, selection of Affimers by phage display and phage ELISA against the kinase domains of all Group II PAK proteins was as previously described^{8,9}. Briefly, biotinylated PAK5 kinase domain (426–719)(EZ-Link NHS-Biotin, Thermo Scientific) was immobilised on blocked (2x blocking buffer, Sigma) streptavidin wells. The Affimer phage library was applied for 2 h and unbound phage removed by PBS-T washes (27 times). Bound phage were eluted in a two-phase step, firstly with 0.2 M Glycine pH 2.2 neutralised with 15 mL of 1 M Tris-HCl, pH 9.1 and then 7.18 M Triethylamine, pH 11 neutralised with 1 M Tris-HCl, pH 7. Three panning rounds were undertaken and after the final panning round 24 randomly picked colonies were used in phage ELISA with positive clones sent for sequencing. The 20 unique sequences were cloned into pET11 using Affimer-His primers (Supplementary Table 1). PAK5-binding Affimers were produced in BL21 STARTM (DE3) E. coli (Life Technologies, Invitrogen) and affinity purified using Ni-NTA resin. The cross-reactivity against the kinase domains of all Group II PAK proteins was determined by phage ELISA^{8,9,25}.

Kinase assay

Kinase assay was performed as described by Cotteret et al.,⁴⁵. All proteins were dialyzed into kinase buffer (25 mM HEPES pH 7.3, 50 mM KCl, 10 mM MgCl₂, 0.1% Triton X-100, 1 mM DTT). Reactions consisted of 20 μg GST-BAD, 500 μM ATP, varying amounts of Affimers (0.5, 2.5, 10 μg) and were initiated by the addition of 2.5 μg PAK5 kinase domain. Reactions were run for 20 min at 30°C and terminated by addition of 4x LBS buffers containing 1 mM DTT. Phosphorylation of GST-BAD was assessed by immunoblotting for phosphorylated S112 as described above using 10 μL of the terminated reaction mixture.

Crystallography

Purified PAK5-Af17 protein was immobilised onto Ni²⁺-NTA beads and incubated with cleared tagless PAK5 lysates overnight at 4°C. The beads were washed with wash buffer (20 mM HEPES (pH 7.5), 150 mM NaCl, 10 mM MgCl₂, 20 mM Imidazole, 0.5% glycerol), and the complex eluted using elution buffer (20 mM HEPES (pH 7.5), 150 mM NaCl, 10 mM MgCl₂, 300 mM Imidazole, 0.5% glycerol). The complex was further purified and buffer exchanged into 20 mM HEPES (pH 8.0), 150 mM NaCl, 5 mM MgCl₂ using size exclusion chromatography using a HiLoad 26/600 Superdex 200 pg column (Cytiva). The PAK5:PAK5-Af17 complex was concentrated to 40 mg/mL and inputting into crystal trials using the high throughput NT8 LCP drop setter (Formulatrix). PAK5:PAK5-Af17 crystals were obtained from the Morpheus Screen 0.12 M Alcohols (0.2 M 1,6-Hexanediol, 0.2 M 1-Butanol, 0.2 M 1,2-Propanediol, 0.2 M 2-Propanol, 0.2 M 1,4-Butanediol, 0.2 M 1,3-Propanediol), 0.1 M Buffer System 2 (1.0 M Sodium HEPES, MOPS) pH 7.5, 37.5% precipitant (M1K3350) by sitting drop vapor diffusion. Crystals were flash-cooled in 100% mother liquor. X-ray diffraction data for the PAK5:PAK5-Af17 complexes were recorded on beamline I04-1 (Wavelength 0.9795 Å) at the Diamond Light at 100 K. Data collection statistics are reported in Supplementary Table 5. Diffraction data were processed and scaled with the Xia2 suite of programs⁹⁰. The PAK5:PAK5-Af17 structure was determined by molecular replacement with the PAK5 structure (PDB:2F57) and an Affimer structure extracted from (PDB:7NY8) excluding the variable regions as the initial search models in the program Phaser.⁹⁰ Structures were refined using REFMAC5,⁹¹ followed by iterative cycles of manual model building using COOT.⁹² The PAK5:PAK5-Af17 structure has been deposited with the PDB code 8C12.

Biacore surface plasmon resonance (SPR)

SPR experiments were performed on a Biacore 1K+ instrument (Cytiva) in kinase buffer +0.05% (v/v) tween 20. Avitag biotinylated PAK5 protein was immobilized on a streptavidin (SA) sensor chip (Cytiva) to ~300RUs. The reference flow cell was un-derivatized. Binding of Affimers was analyzed using 3-min injections over a 2-fold dilution series from 800nM to 3.1 nM at 30 μL/min flow-rate and 25°C. Surfaces were regenerated between cycles using a 1 min injection of NaHCO₃ 0.1M. Data were processed using Evaluation software version 5.0.16.21762 using “double referencing” with subtraction of the signal from the reference flow-cell and from a buffer injection over the active surface. Affinity values were determined by fitting equilibrium binding signals versus concentration for a 1:1 interaction model.

QUANTIFICATION AND STATISTICAL ANALYSIS

Statistical analyses were carried out in GraphPad Prism 8.00 software (GraphPad Software, La Jolla, CA), with robust Z scores $Z = (x_i - \bar{x})/MAD$ and Z scores $Z = (x_i - \bar{x})/SD$ -calculated in Microsoft Excel (Redmond, WA) as per the formulae in Birmingham et al. (2009)⁴⁰. Statistical assumptions of equal variance for one-way ANOVA were tested with Brown-Forsythe tests.

Cell Reports, Volume 42

Supplemental information

**Affimer-mediated locking of p21-activated
kinase 5 in an intermediate activation
state results in kinase inhibition**

Heather L. Martin, Amy L. Turner, Julie Higgins, Anna A. Tang, Christian Tiede, Thomas Taylor, Sitthinon Siripanthong, Thomas L. Adams, Iain W. Manfield, Sandra M. Bell, Ewan E. Morrison, Jacquelyn Bond, Chi H. Trinh, Carolyn D. Hurst, Margaret A. Knowles, Richard W. Bayliss, and Darren C. Tomlinson

SUPPLEMENTARY DATA

Table S1. Parameters used to identify cell-cycle phase. Images taken with the PerkinElmer Operetta were analysed using the Columbus software in a sequential manner using the methodology and thresholds outlined. * populations are summed to form M phase population.

Input Population	Channel and Method used	Thresholds	Output population
All cells	DAPI, Method B	Common threshold = 0.6; Area >30 μm^2 ; Border objects excluded	All whole cells
All whole cells	AlexaFluor 546, Nuclear Intensity	Intensity Maximum >500 AND Intensity Mean >350	Phosphohistone H3 positive cells
Phosphohistone H3 positive cells	AlexaFluor 546, Nuclear size	Nuclear Area >200 μm^2	Prophase cells*
Phosphohistone H3 positive cells	AlexaFluor 546, Nuclear size	Nuclear Area <200 μm^2 Population modified by clustering by distance of 20px	Metaphase and anaphase cells
Metaphase and anaphase cells	AlexaFluor 546, Region Area and roundness	100 μm^2 < Region Area <200 μm^2 ; Region Roundness < 0.7	Anaphase cells*
Metaphase and anaphase cells	AlexaFluor 546, Region Area and roundness	Region Area >100 μm^2 ; Region Roundness 0.7	Metaphase cells*
All whole cells	AlexaFluor 546, Nuclear Intensity	Intensity Maximum \leq 500 AND Intensity Mean \leq 350	Phosphohistone H3 negative cells
Phosphohistone H3 negative cells	DAPI, Nuclear intensity and size	Nuclear Area <100 μm^2 AND Intensity Mean >7000 Population modified by clustering by distance of 20px	Telophase and apoptotic cells
Telophase and apoptotic cells	DAPI, Region Area	Region Area >150 μm^2	Telophase cells*
Telophase and apoptotic cells	DAPI, Region Area	Region Area <150 μm^2	Apoptotic cells

Phosphohistone H3 negative cells)	DAPI, Nuclear intensity and size	Nuclear Area >100 μm^2 AND Intensity Mean <7000	Non mitotic or apoptotic cells
Non mitotic or apoptotic cells	AlexaFluor 488, Nuclear Intensity	Intensity Maximum >400 AND Intensity Mean >300	S phase cells
Non mitotic or apoptotic cells	AlexaFluor 488, Nuclear Intensity	Intensity Maximum <400 AND Intensity Mean <300 Nuclear spots detected by method A	G phase cells
G phase cells	AlexaFluor 633; Number of Nuclear spots (detected by method A, relative spot intensity >0.020 and splitting coefficient = 0.8)	Number of spots ≤ 2	G0 phase cells
G phase cells	AlexaFluor 633; Number of Nuclear spots (detected by method A, relative spot intensity >0.020 and splitting coefficient = 0.8)	Number of spots >2	G1 and 2 phase cells
G1 and G2 phase cells	DAPI and AlexaFluor 633, Nuclear intensity and number of Nuclear spots	Nuclear intensity > 1500; Number of spots >10	G2 phase cells
G1 phase cells	All cells – SUM (All other populations)		

Table S2. Strictly standardized mean differences (SSMDs) for the three controls across the seven primary outputs. SSMDs were calculated as described in the methods and interpreted as outlined by Bray *et al.*,¹. Numbers in bold represent good controls when tested at the strong control level, whilst the remaining controls are good controls when measured at the moderate control level.

Control	Phenotype						
	Cell number	% Apoptotic cells	% G0 phase cells	% G1 phase cells	% S phase cells	% G2 phase cells	% M phase cells
<i>PLK1</i>	-3.48	4.22	-	-	-	-	2.45
<i>PSMB1</i>	-1.01	-	-	-	-	-1.27	-1.78
<i>POLA1</i>	-0.97	-	-	2.51	-1.20	-1.93	-
<i>CCNE1</i>	-3.06	-	2.09	2.30	-2.91	-2.80	-1.52

Table S4. Primers used in this study

Primer name	Primer sequence 5' – 3'
PAK5 to pET11 F	ATAGCTAGCATGAGGGTGTCCCATGAACAG
PAK5 to pET11 R	ATAATAGCGGCCCGCCCTGTATTGTCTCATGAGGG
PAK5 Tagless R	ATAATAGCGGCCCGCTTACCTGTATTGTCTCATGAGGG
PAK 4 to BAP and His Tag F	AAGAAGGAGATATACATATGCGAGTATCCCATGAGCAG
PAK 4 to BAP and His Tag R	TCAAAAATGTCGTTTCAGGCCCTCTGGTGCGGTTCTGGC
PAK 5 to BAP and His Tag F	AAGAAGGAGATATACATATGAGGGTGTCCCATGAAC
PAK 5 to BAP and His Tag R	TCAAAAATGTCGTTTCAGGCCCTGTATTGTCTCATGAGG
PAK 6 to BAP and His Tag F	AAGAAGGAGATATACATATGGTGACACATGAGCAGTTC
PAK 6 to BAP and His Tag R	TCAAAAATGTCGTTTCAGGCCGGTGGAGGTCTGCTTTC
BAP Tag to pET11 F	GGCCTGAACGACATTTTTGAAG
BAP Tag to pET11 R	CATATGTATATCTCCTTCTTAAAG
PAK4 A683G F (K526R)	GCCACCCCTCAAAGCCATGAGGATGATTCCGGGACAACCTG
PAK4 A683G R (K526R)	CAGGTTGTCCCGAATCATCCTCATGGCTTTGAGGGGTGGC
PAK6 A680G F (K610R)	GACTCCCCAGTGCAAGCCATGAGGAGGCTCCGGGACAGCC
PAK6 A680G F (K610R)	GGCTGTCCCGGAGCCTCCTCATGGCTTGCACTGGGGAGTC
Affimer from pDHis to pET11 F	ATGGCTAGCAACTCCCTGGAAATCGAAG
Affimer from pDHis to pET11 R	TACCCTAGTGGTGATGATGGTGATGC
Affimer from pDHis to pCMV6-tGFP F	TATATGCGATCGCCATGGGTAACGAAAACCTCCCTG
Affimer from pDHis to pCMV6-tGFP R	AATACGCGTAGCGTCACCAACCGGTTTG

Table S4. X-Ray crystallographic data collection and refinement statistics for PAK5-Af17:PAK5 complex. Values given in parentheses correspond to those in the outermost shell of the resolution range.

Data set	PAK5:PAK5-Af17
Space Group	P2 ₁ 2 ₁ 2 ₁
High Resolution limit (Å)	1.55 (4.20, 1.55)
Low Resolution limit (Å)	53.21 (53.20, 1.58)
Unit-cell parameters	a = 57.36 Å b = 58.31 Å c = 129.47 Å
	$\alpha = 90.0^\circ \beta = 90.0^\circ \gamma = 90.0^\circ$
No. of observed reflections	856200 (43336, 41120)
No. of unique reflections	64001 (3476, 3075)
Multiplicity	13.4 (12.5, 13.4)
Completeness (%)	100.0 (100.0, 97.8)
I/ σ	16.3 (75.7, 0.3)
R _{merge} (I+/-)	0.055 (0.034, 2.735)
R _{pim} (I+/-)	0.022 (0.014, 1.087)
CC (1/2)	0.999 (0.997, 0.577)
R factor (%)	19.7
R _{free} (%)†	23.4
No. of protein non-H atoms	3053
No. of water molecules	195
R.m.s.d bond lengths (Å) ξ	0.0134
R.m.s.d bond angles (°) ξ	1.65
<u>Average overall B factor (Å²)</u>	
Protein	43.7
Water	46.4
<u>Residues in the favoured region of Ramachandran plot (%) \ddagger</u>	
Favoured region	97.9
Outliers	0
<u>PDB code</u>	8C12

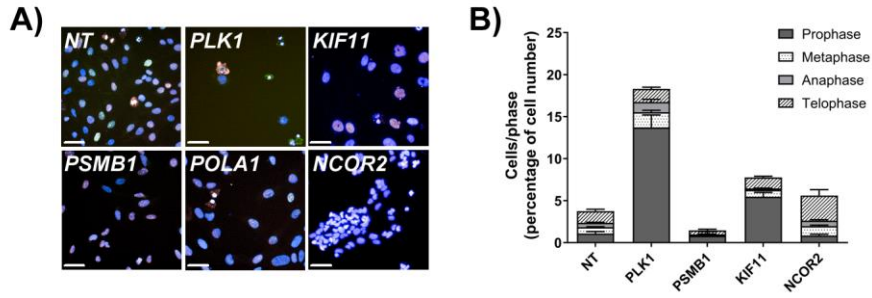


Figure S1. Validation of novel high content imaging analysis of cell cycle. Representative images of cell phenotypes seen with non-targeting (NT), *PLK1*, *KIF11*, *PSMB1*, *POLA1* and *NCOR2* siRNA (**A**) and their effects on the percentage of cells in each of the individual subdivisions of mitosis (**B**) Data are mean \pm SEM, n= 3 independent experiments, scale bars are 50 μ m.

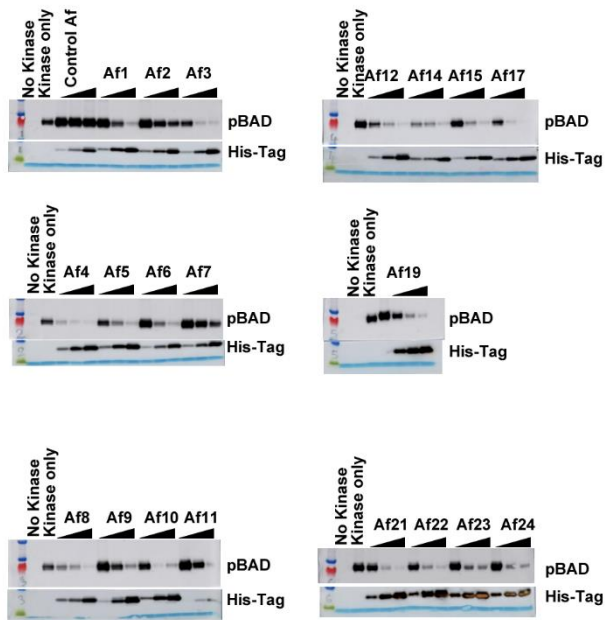


Figure S2. Inhibitory and characterisation of PAK5-binding Affimers. Blots from which the representative blots for the four selected Affimers shown in Figure 3B were taken, showing the ability of the 20 PAK5-binding Affimers to inhibit PAK5-mediated phosphorylation of BAD at different w/w ratios in an *in vitro* kinase assay and compared to a control Affimer (that binds yeast SUMO protein).

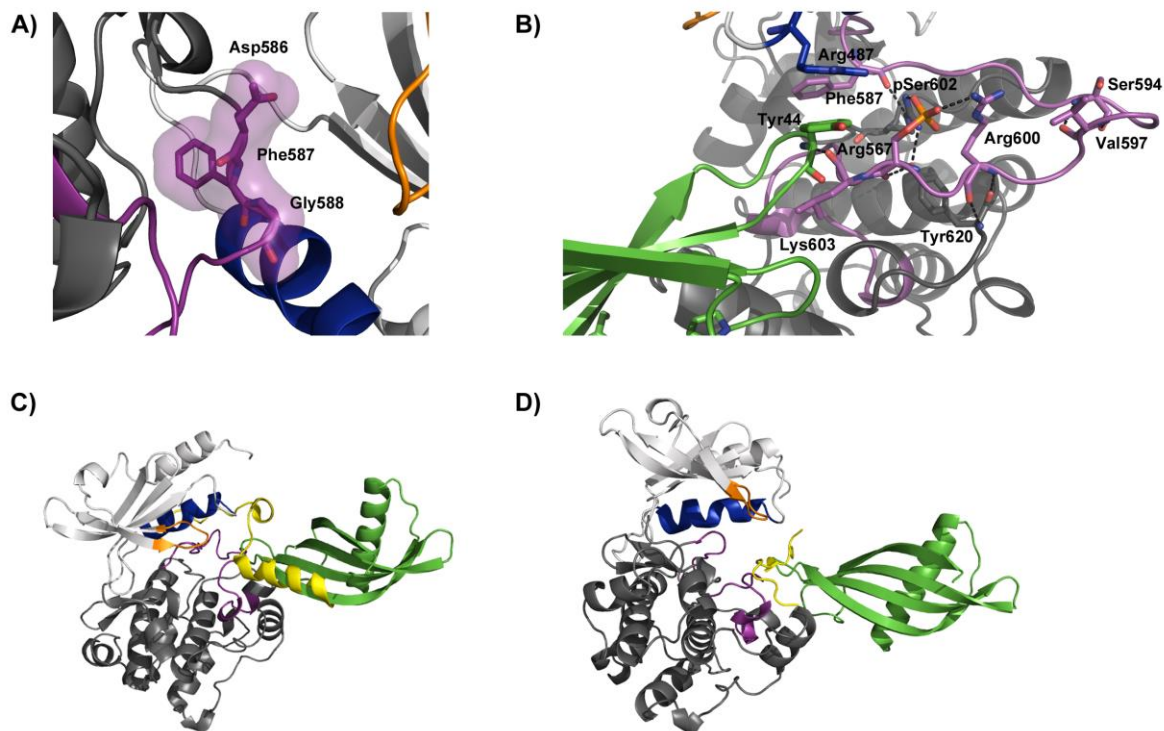


Figure S3. Additional structural features of PAK5-Af17:PAK5 complex and comparison to other structures. The DFG motif is shown as purple sticks surrounded by a surface. It resides in the DFG-in conformation with Phe587 buried between the N- and C-terminal lobes (A). pSer602 is monophosphorylated and maintains an active H-bonding network within the activation loop in the presence of PAK5-Af17 (B). Overlaid structures of the Aurora A binding N-Myc extracted from PDB code: 5G1X (yellow cartoon) with the PAK5:PAK5-Af17 complex (PAK5-Af17 in green cartoon) (C). Overlaid structures of the PAK4 binding Inka1 peptide extracted from PDB code: 4XBU (yellow cartoon) with the PAK5:PAK5-Af17 complex (PAK5-Af17 in green cartoon) (D).

References

1. Bray, M.A.C., A.; (2012). Advanced Assay Development Guidelines for Image-Based High Content Screening and Analysis. In G.-E.N. Sittampalam GS, Arkin M, et al. ed.